11-2019

Enhancing Single Walled Carbon Nanotube Deposition For The Study Of Extracellular Analytes

Joseph A. Stapleton
University of Nebraska-Lincoln, JStapleton346@gmail.com

ENHANCING SINGLE WALLED CARBON NANOTUBE DEPOSITION FOR THE STUDY OF EXTRACELLULAR ANALYTES

By

Joseph A. Stapleton

A THESIS

Presented to the Faculty of

The Graduate College at the University of Nebraska

In Partial Fulfillment of Requirements

For the Degree of Master of Science

Major: Agricultural & Biological Systems Engineering

Under the Supervision of Professor Nicole M. Iverson

Lincoln, NE

November 2019

ENHANCING SINGLE WALLED CARBON NANOTUBE DEPOSITION FOR THE STUDY OF EXTRACELLULAR ANALYTES

Joseph A. Stapleton, M.S.

University of Nebraska, 2019

Advisor: Nicole M. Iverson

Extracellular signaling is a dynamic process responsible for coordinating large scale biological processes. As such, understanding extracellular signaling is important to our determination of normal function and pathophysiological development. High resolution spatial and temporal information are critical to completely understanding these processes. Unfortunately, current methods of detection are lacking in either spatial or temporal resolution of extracellular products, limiting researchers' ability to understand complex biological processes. A new group of sensors based on fluorescent single walled carbon nanotubes (SWNT) have shown the potential to provide both high quality spatial and temporal resolution for the sensing of analytes. However, while SWNT has already been used extensively as an intracellular probe, it has seldom been used for intercellular monitoring. In the few instances that SWNT has been used to form extracellular sensor arrays the deposition method has relied on electrostatic or non-specific interactions and is not well characterized. Herein a new method of SWNT deposition based on the avidin-biotin bond was developed, where biotin activity was imparted to SWNT via coupling to its DNA wrapping and avidin was covalently immobilized on the surface of a glass slide. The method of SWNT immobilization produced a twofold enhancement in SWNT deposition over the current standard without negatively impacting SWNT spectral

properties, distribution, response time, or degradation rates. These results indicate the effectiveness of this method for increasing SWNT deposition and provide a simple pathway for enhancing the deposition of DNA-SWNT complexes.

ACKNOWLEDGEMENTS

To my advisor Dr. Iverson, you gave me a chance some four years ago when I joined your lab as an undergraduate. At that time I lacked direction, but under your careful guidance I learned the wonders of research and became the Engineer that I am today. The motivation, knowledge, and patience that you supplied made my Master's work possible. I could not have asked for a better advisor and mentor.

To my committee members, Dr. Angela K. Pannier, Dr. Yufeng Ge, and Dr. David Jones, thank you for continually pushing me to produce the best work possible. Your insightful questions, commentary, and suggestions made this thesis possible.

To my fellow Iverson lab members both past and present, I would not have been able to accomplish this work without you. You have served as valuable sources of knowledge and dear friends throughout the course of my time here. This lab has become like a second home to me and I will miss it dearly.

To my girlfriend Ali, you have been on this journey with me since Freshman year of college and what a great journey it has been. After helping me to get through undergraduate school you stayed with me in Lincoln and put your dreams of opening your own dance studio on pause. For that I can never repay you. You put up with my long nights and weekends of work without complaining, and all the while you helped me keep my sanity, one smile and word of encouragement at a time. Without you I would not have been able to accomplish my Master's work. I can't wait to see what our life together holds in store for us.

Finally, to my parents, Mom and Dad, thank you for your lifelong support of me. Your lives have taught me the value of hard work and compassion for others. Your gentle encouragement has helped me to preserver in the face of what sometimes seemed to be overwhelming odds. Without you I would not have been able to complete this work. I love you both.

LIST OF ABBREVIATIONS

3-GPTMS	3-glycidoxypropyltrimethoxysilane
AA	Ascorbic acid
AFM	Atomic force microscopy
ATP	Adenosine triphosphate
ATPES	3-aminopropyltriethoxysilane
BA-PhO-Dex	Boronic acid-substituted phenoxy-dextran
BH_4	Tetrahydrobiopterin
BSA	Bovine serum albumin
B-SWNT	Biotinylated SWNT
CaM	Calmodulin
cGMP	Cyclic guanosine monophosphate
cNOS	Constitutive NOS
CO	Carbon monoxide
CVD	Chemical vapor deposition
DA	Dopamine
DAF-2	4,5-diaminofluorescein
DAF-2T	DAF-2 triazole
DAP-DEX	3,4-diaminophenylfunctionalized dextran
DHA	Dehydroascorbic acid
DNA	Deoxyribonucleic acid
EDRF	Endothelium-derived relaxing factor

eNOS	Endothelial NOS
EPR	Electron paramagnetic resonance spectroscopy
FAD	Flavin adenine dinucleotide
FAM	Fluorescein amidide
$[Fe(DTCS)_3]^{3-}$	Tris(n-(dithiocarboxy)sarcosine)iron(iii)
FMN	Flavin-mononucleotide
Fmoc-Phe-PPEG8	Fmoc l-phenylalanine
FWHM	Full width half max
GFP	Green fluorescent protein
GTP	Guanosine triphosphate
H_2O_2	Hydrogen peroxide
HABA	4'-hydroxyazobenzene-2-carboxylic acid
HEPES buffer	4-(2-hydroxyethyl)piperazine-1-ethanesulfonic acid
HiPco	High-pressure carbon monoxide
HIV	Human immunodeficiency virus
HRP	Horseradish peroxidase
HUVEC	Human umbilical vein endothelial cells
IgD	Human immunoglobin D
IgG	Human immunoglobin G
IgG2a	Rat imunoglobin G2a
IgM	Mouse immunoglobin M
iNOS	Inducible NOS
IR	Infrared

L-Arg	L-arginine
L-Cit	L-citrulline
LDL	Low-density lipoproteins
miRNA	MicroRNA
NADP	Nicotinamide adenine dinucleotide phosphate
NADPH	Dihydronicotinamide-adenine dinucleotide phosphate
NB-SWNT	Non-biotinylated-SWNT
NE	Norepinephrine
NED	N-1-napthylethylenediamine dihydrochloride
NHS	N-hydroxysuccinimide esters
nIR	Near infrared
nNOS	Neuronal NOS
NO	Nitric oxide
NOS	Nitric oxide synthase
PBS	Phosphate-buffered saline
PCR	Polymerase chain reaction
PE-CVD	Plasma enhanced CVD
PEG	Polyethylene glycol
PLPEG	Phospholipid-polyethylene glycol
PMMA	Poly (methyl methacrylate)
PP_i	Pyrophosphate
PS	Polystyrene
QDs	Quantum dots

RAP-1	Ras-associated protein-1
RITC-PEG-RITC	Rhodamine isothiocyanate-difunctionalized poly(ethylene glycol)
RNA	Ribonucleic acid
RNS	Reactive nitrogen species
ROS	Reactive oxygen species
SDBS	Sodium dodecyl benzene sulfonate
SDS	Sodium dodecyl sulfate
sGC	Soluble guanylyl cyclase
SNPs	Single nucleotide polymorphisms
ssDNA	Single-stranded DNA
SWNT	Single walled carbon nanotubes
TRIS	Tris (hydroxymethyl) aminomethane
UPS system	Ultraviolet photoelectron spectroscopy
UV-Vis	Ultraviolet-visible
XPS	X-ray photoelectron spectroscopy

TABLE OF CONTENTS

LIST OF FIGURES

LIST OF TABLES

CHAPTER 1

Thesis Introduction, Background, Objectives

1.1 Introduction

Fluorescent single walled carbon nanotubes (SWNT) are seamless roles of graphene that have demonstrated great diagnostic potential within the biomedical field [1-7]. Although the use of SWNT to detect biological molecules has many advantages, there are still impediments that must be overcome to make these sensors more useful for analyte detection. Currently, one of SWNT's greatest advantages, the ability to form a high-density sensor array for high definition spatio-temporal visualization of extracellular analytes, lacks proper characterization and relies almost entirely on electrostatic or non-specific interactions [8-10]. Electrostatic and non-specific interactions are plagued by their instability and inconsistent loading [11]. **For SWNT to be a viable reporter of extracellular analytes, further characterization of current deposition approaches and the development of new methods for the immobilization of SWNT which employ greater specificity must be developed**. One mechanism which could be used to increase SWNT loading and specificity is the avidin-biotin interaction. The avidin-biotin interaction is the strongest known non-covalent bond and also enjoys high specificity [12]. Moreover, biotin can be easily coupled to DNA, which is one of the most common and versatile wrappings for SWNT sensor complexes [13, 14]. Additionally, avidin can be covalently bound to glass substrates, through simple silane chemistry [15]. Increases in SWNT loading due to the application of the avidin-biotin bond could have an immediate impact on critical elements related to SWNT sensors including: cost savings

due to increases in SWNT loading efficiency, decreased intensity of laser emissions necessary for sensor functioning, which may extend the life of the laser and decrease its effects on the sample, and decreased exposure time, allowing for increased data collection and less time for cell cultures to spend outside of the incubator. A proof of concept using the avidin-biotin interaction with a representative and relevant DNA-SWNT complex would be of great benefit to the field. The nitric oxide (NO) sensing SWNT sensor is an ideal candidate for proof of concept work. The NO sensing SWNT sensor possesses a simple DNA wrapping that is representative of other DNA-SWNT sensors while its target analyte, NO, is a highly versatile signaling molecule with a role in numerous biological systems including the vasculature, nervous, and immune systems [16-18]. NO has also been implicated in a multitude of pathophysiological states, where its effects appear to be highly dependent upon its local concentration and duration of aberrant expression, including the development of cardiovascular diseases, neurodegenerative diseases, inflammatory diseases, and carcinogenesis [19-44]. Unfortunately, a lack of adequate sensors for the detection of extracellular NO signaling has hindered the study of these disease states. Due to the promising properties of SWNT, the need to develop improved surfaces for SWNT deposition, and its immediate application to the field of NO research, the objectives of this thesis are to **1) Evaluate the ability of DNA-SWNT complexes to bear a biotin moiety without damaging SWNT spectral properties, 2) Develop and characterize a new method of SWNT deposition which utilizes the avidin-biotin interaction, and 3) Determine if enhanced SWNT deposition could be realized using the avidin-biotin process without damaging SWNT's previously held properties**. To introduce these objectives, Chapter 1 will

cover detailed background information on SWNT as optical biosensors, current DNA-SWNT complex deposition methods, and NO's role in biomedical systems.

1.2 Single Walled Carbon Nanotubes

SWNT are hollow cylinders of carbon atoms occupying a distinctive honeycomb lattice, which are 0.5-2 nm in diameter, and range in length from 50 nm to several centimeters depending upon the method of preparation [45-48]. Since the discovery of SWNT in 1993 by Iijima and Ichihashi, considerable attention has been paid to SWNT's unique and often extraordinary tensile and compressive properties, thermal and electrical conductivity, and optical phenomena [49-58]. For example, SWNT is one of the strongest known materials when normalized to its diameter, with a Young's modulus of approximately 1 tera pascal (TPa) compared to steel's 190 to 215 GPa [59, 60]. Moreover, the theoretical thermal conductivity of SWNT is 6000 W/mK which greatly exceeds that of diamonds (~1000 W/mK)[61, 62].

In addition to SWNT's many applications in mechanical and electrical systems, SWNT has also been recognized for its potential usefulness in biological and biomedical applications including cell tracking, optic labeling, delivery of biologically relevant signaling molecules, and matrix enhancement [63-68]. Of particular interest are SWNT's inherent near infrared fluorescent properties, ability to be wrapped by surfactants, polymers, and single stranded DNA (ssDNA), and when properly prepared, their ability to detect biologically relevant molecules. To date SWNT has been used to fluorescently

detect genetic material, proteins, signaling molecules, lipids, genotoxic elements, antibodies, and several other biologically relevant molecules [1-4, 7-10, 69-84]. Of distinct note are those sensors capable of detecting the reactive oxygen and nitrogen (ROS/RNS) species NO and hydrogen peroxide (H_2O_2), which have suffered from a lack of appropriate real time *in vitro/in vivo* sensor platforms due to their short half-lives (H_2O_2 < 50 ms, NO < 1.8 ms) and high reactivity [85-89]. The ability of SWNT to sense these molecules in close proximity to their sources could allow for a more accurate real time understanding of cellular signaling dynamics.

1.2.1 Generating Single Walled Carbon Nanotubes

Before SWNT can be used as an optical reporter it must be produced. A number of techniques have been developed for the production of single walled carbon nanotubes including electric arc discharge, laser ablation, chemical vapor deposition, and high-pressure carbon monoxide deposition methods.

The electric arc technique is one of the oldest techniques for producing relatively large quantities of SWNT [90]. Originally used by Smalley and Haufler to generate C_{60} Buckminsterfullerenes (Bucky balls), the technique was later co-opted to generate SWNT [91]. Usually performed under helium, this method employs an arc discharge designed to strike a combination of metallic catalysts and graphite powder, where the graphite powder serves as a carbon source. Metallic catalysts used include, but are not limited to, Ni-Co, Co-Y, and Ni-Y at various atomic percentages [92]. The discharge is generated by

sustaining (~2 min) a large current (100 A) between the graphite cathode and the anode, which produces a voltage drop of 30V between the electrodes [90]. The discharge repeatedly vaporizes the carbon/metallic composite which allows the metallic catalysts to serve as a nucleation site for the production of SWNT [93]. Following discharge, a web-like soot that contains SWNT is produced [94]. The product is typically composed of many different diameters of SWNT, but it is possible to vary the characteristics of the carbon nanotubes by varying the current, pressure, and nature of the catalyst within the chamber [95]. The careful control of the chamber parameters and subsequent purification can produce SWNT yields as high as 80% [90, 96, 97].

Laser ablation is another method for the production of SWNT. Rather than using an arc discharge, laser ablation's goal is to vaporize graphene/metal catalyst complexes using a high intensity laser and allow for the formation of SWNT upon condensation [98-100]. There are currently two methods for generating SWNT via laser ablation, which are classified by the method of laser operation: (1) a pulsing laser option and (2) a continuous laser option [99-101]. When a pulsing laser is used it is common to keep the reaction chamber that is housing the graphite/metal complex at ~1200 °C, which is close to the graphite vaporization zone [100, 102]. Upon exposure to the pulsed laser light the graphite/SWNT complex achieves enough energy to become vaporized, with the metal serving as a nucleation site [98]. However, when a constant laser source is used there is no need to keep the camber at a high temperature, instead a powerful (250 W) laser is directed at rods of the graphene/metal complex, allowing them to reach vaporization temperatures without the aid of an oven [99]. In both cases argon gas is generally flowed through the system to transport the vaporized substrate to a holding chamber where it can

condense into SWNT and be more readily collected (Figure 1-1) [99, 100]. Using this method, as much as 20% of the mass from the original graphene/metal can be recouped in the final product, while the final product itself has a purity of ~ 80% SWNT [99, 100]. Although this method generally produces SWNT of many diameters, the diameter distribution can be controlled by varying the metallic catalyst, temperature, and gas flow velocity [103].

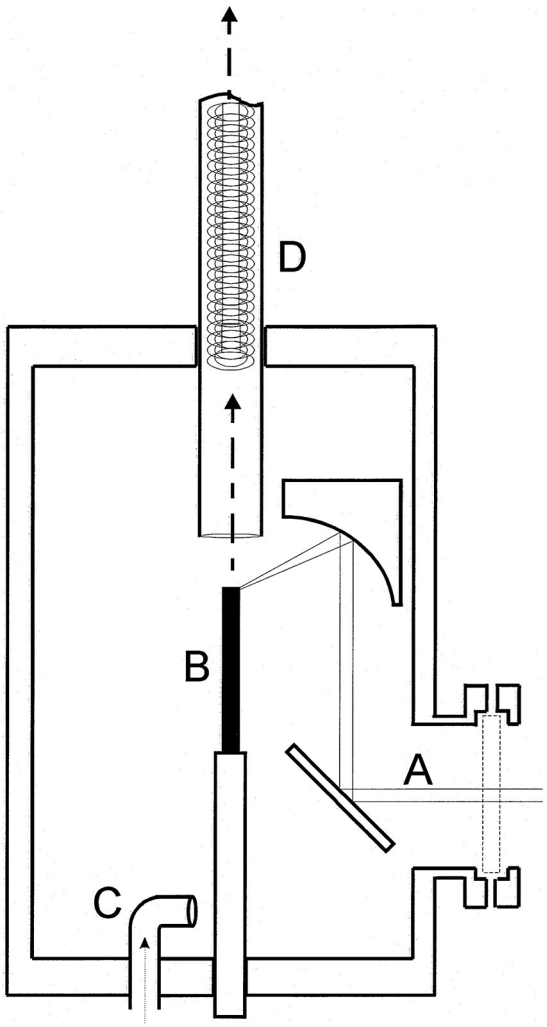

Figure 1-1: Generation of SWNT via laser ablation. The laser beam (A) is maneuvered into the evaporation chamber and focused onto the graphite/metal composite target cylinder (B). Inert gas is run through a nozzle (C). Products are collected on the Cu-wire scaffold inside a quartz tube (D) leading to the filter and pumping unit. Reprinted from Maser et al. with permission from Chemical Physical Letters [99].

Chemical vapor deposition (CVD) utilizes a thin catalyst/support material to generate SWNT under high temperatures. Catalyst materials that have been frequently used include Fe, Ni, Co, and Mo with a support layer of Al, SiO_2, or Mg [104-107]. Support material can either be impregnated with the metal catalyst and used as a fine powder (e.g. Fe_2O_3/Al) [108], or the two can be kept sperate by forming a support and catalytic layer (e.g. Al/Ni support/catalytic layer) [109]. When it is desired that the two layers be kept separate, deposition of the catalytic layer and support layer are generally produced through beam sputtering or electron beam evaporation [109, 110]. The support/catalyst is then placed in a chamber that is subsequently purged and filled with an inert gas (e.g. H_2). The reaction chamber is subsequently heated to high temperatures (800 -1200 °C) which causes the formation of oxidized support clusters (e.g. $Al_2O_{3)}$, which in turn provide support for the formation of metallic nanoparticles. Any number of carbon containing gases are then flowed through the chamber including CO, $CH_{4,}$ C_2H_4, C_2H_2, or benzene at ~ 100 torr for 60 min [104-109, 111-118]. The metallic nanoparticles again act as nucleation sites for the formation of SWNT while the carbon containing gas serves as the carbon source for the growth of SWNT. Many techniques have been developed to augment the CVD process and decrease the prohibitively high working temperatures, including plasma enhanced CVD (PE-CVD), which achieves lower reaction temperatures by ionizing the reaction gases causing increased reactivity at the catalytic surface [110]. Using the CVD method purities as high as 90% can be achieved [119].

The high-pressure carbon monoxide (HiPco) process represents the culmination of a series of methods focused on pyrolysis of SWNT precursors [118, 120]. In the HiPco

process, SWNT is generated by passing carbon monoxide (CO) and a small amount of iron pentacarbonyl ($Fe(CO)_5$) through a high pressure (30 atm), high temperature (1050°C) reactor (Figure 1-2). Upon reaching temperature, $Fe(CO)_5$ undergoes thermal decomposition and forms iron clusters in the in the gas phase. The iron clusters can then act as nucleation sites for the SWNT to grow via a CO disproportionation reaction [114]. The nucleated iron clusters are then carried out of the reaction chamber to a cooling/collection area where the SWNT can continue developing. The HiPco process is the only gas phase continuous process, which allows it to excel at high production rates (450 mg/h) and high purity (97 mol%) [114].

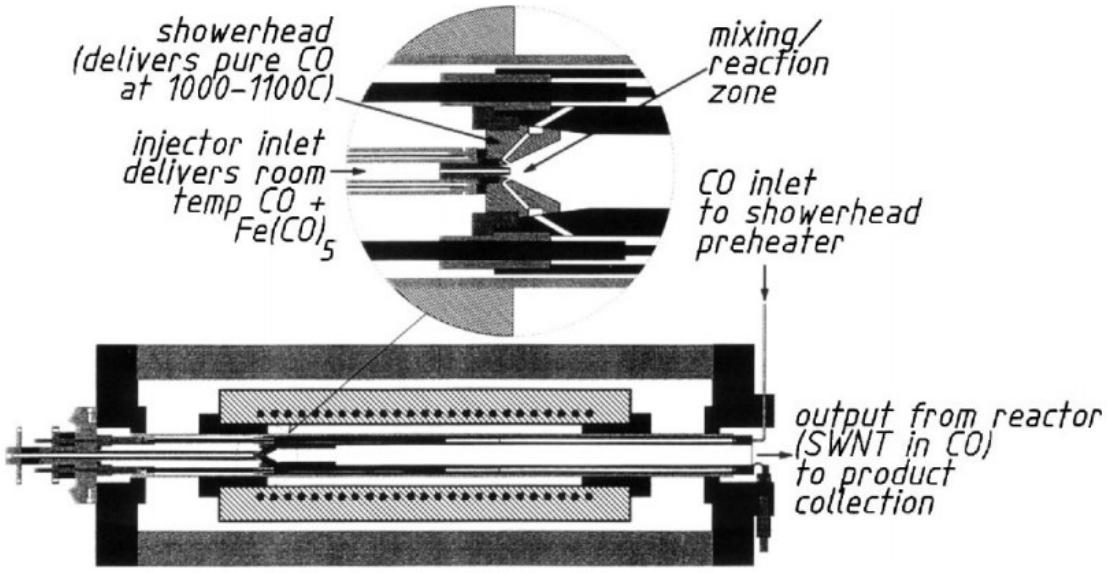

Figure 1-2: Production of SWNT via a HiPco reactor, with the reaction region shown enlarged. Room temperature CO and $Fe(CO)_5$ are fed into the reactor at the left. Meanwhile, a separate CO source is rapidly heated to ~ 1050 °C. The hot CO is then delivered to the room temperature CO and $Fe(CO)_5$ via a shower head, rapidly heating the $Fe(CO)_5$ and encouraging its decomposition. Upon decomposition, $Fe(CO)_n$ serves as a nucleation site for SWNT growth. The nucleated particles are shuttled out of the reactor where they can finish growing and be collected. Reprinted from Bronikowski et al. with permission form the Journal of Vacuum Science and Technology A [114].

1.2.2 Fluorescent Theory

SWNT show heterogenous optical and electrical properties upon production that are highly dependent upon their chiral angle [121, 122]. Often denoted with the *n,m* notation, chiral angle describes the orientation of a graphene sheet should it be rolled into a nanotube (Figure 1-3). Depending upon the chiral angle, SWNT can present as either a semi-conductor or metallic material [123]. The properties of the SWNT (semi-conductor or metallic) can be predicted from the following equation: when $|n - m| = 3q$, where q is an integer, the nanotube is metallic and in all other cases the SWNT is considered semi-conducting [124]. Unfortunately, as prepared SWNT are generally a mixture of many different SWNT chirality's which are grouped together axially in bundles via van der Waals binding [125, 126]. The dispersion of aggregated SWNT bundles is a challenge for those who want to utilize their individual properties. Not only does aggregation of SWNT perturb the electronic structure of individual nanotubes, but it also prevents the individual study of species based on their chiral angle. It was in pursuit of dispersion that fluorescent single walled carbon nanotubes were discovered. In 2002, *O'Connell et al.* demonstrated that not only could individual SWNT be easily dispersed by sonication with sodium dodecyl sulfate (SDS) micelles, but upon excitation by a 532 nm laser the dispersed semi-conducting varieties of SWNT produced a bright fluorescence in the near infrared range [122].

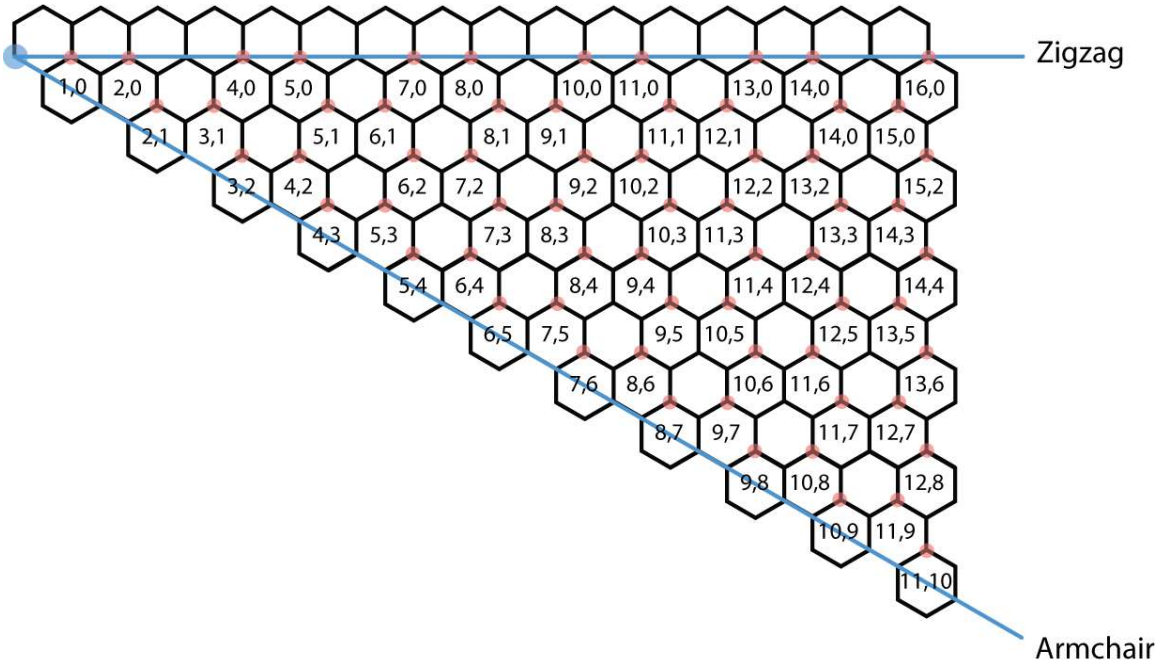

Figure 1-3: Visualizing SWNT chirality's. SWNT can be thought of as a rolled sheet of Graphene. The angle at which the tube is rolled defines the properties of the SWNT (semiconductor or metallic) The n,m notation system is used to define chiral angle of the tube formed by rolling the graphene sheet. when |n-m|=3q, where q is an integer, the nanotube is metallic and was thus not included in this figure. Figure created from work in [121]

Due to their demonstrated ability to undergo band-gap fluorescence, semi-conducting SWNT form the framework for all fluorescent SWNT sensor applications [122]. Fluorescence is generated as a result of the quasi-quantum confinement of electrons along the axis of the nanotube [79]. The electron confinement generates a series of Van Hove peaks which account for SWNT fluorescence [121, 127] (Figure 1-4a). The chirality (and thus the diameter) of the single walled carbon nanotube directly influences the absorption and fluorescence spectra by altering the electron density of states, with peak excitation values ranging from approximately 550-800 nm and corresponding maximum fluorescence ranging from 900-1600 nm [121, 128] (Figure 1-4b). The presence of fluorescent peaks in the infrared is well suited to biological applications.

Infrared signals are known for their ability to penetrate tissue and cell culture beyond that of visible wavelengths while avoiding autofluorescence from typical biological materials such as tissue, blood, and cell culture reagents [129-131]. Unfortunately, unmodified or raw SWNT is not well suited to fluorescent applications. Raw SWNT is hydrophobic and forms dense aggregates in aqueous solution, which prevents the SWNT from fluorescing by altering its electronic structure and prevents the study of individual SWNT species. Furthermore, raw SWNT lacks specificity in its interaction with analytes/ligands preventing its usefulness as a sensor [132, 133]. Covalent modifications to increase solubility were considered and applied, but these methods result in loss or serious damage to the near infrared optical properties of SWNT by necessarily disrupting its quasi-one-dimensional state [124, 134]. Consequentially, a number of non-covalent modifications have been developed to increase hydrophilicity and, in some cases, impart ligand/analyte binding sensitivity. Non-covalent modifications which have been successfully employed include surfactants (SDS micelles), polymers wrappings (Dextran, collagen, etc.), and DNA wrappings [8, 9, 70, 71, 73, 135-137]. Despite initial success with surfactants, more recent single walled carbon nanotube probes have relied heavily on polymers and DNA wrappings which are easily imparted through sonication [136]. DNA wrapping in particular is considered to be a highly ordered process due to hydrophobic interactions and pi stacking between the single walled carbon nanotube and aromatic rings in the wrapping [136]. DNA and polymer wrappings impart several important features to SWNT: 1) The SWNT system becomes hydrophilic, allowing for dispersion in biological systems, 2) The optical properties of the SWNT are preserved because no covalent bonds, which would alter their quasi-one-dimensional state, and 3) Ligand/Analyte specificity is

imparted as a result of wrapping. DNA wrapping can impart ligand specificity for small molecules like NO via steric hinderance, nonradiative energy loss, and redox selectivity [9]. For large molecules like proteins or genetic material DNA can serve as an attachment site for molecules that will interact with the analyte of interest, such as aptamers or microRNA [3, 8, 84]. Binding of the analyte of interest affects the dielectric environment of SWNT and results in a modulation of the fluorescence. For example, the NO specific sensor indicates NO binding with a decrease in fluorescent intensity, while the Ras-associated protein-1 (RAP-1) sensor demonstrates protein binding as an increase in fluorescence, and the recently developed microRNA sensor identifies binding as a blue shift [6, 8, 9]. DNA wrapped SWNT also stand in marked contrast to other infrared probes (Quantum dots, IR dyes) in that they have shown no indication of photobleaching and have remained stable for more than 300 days *in vivo* [5, 138]

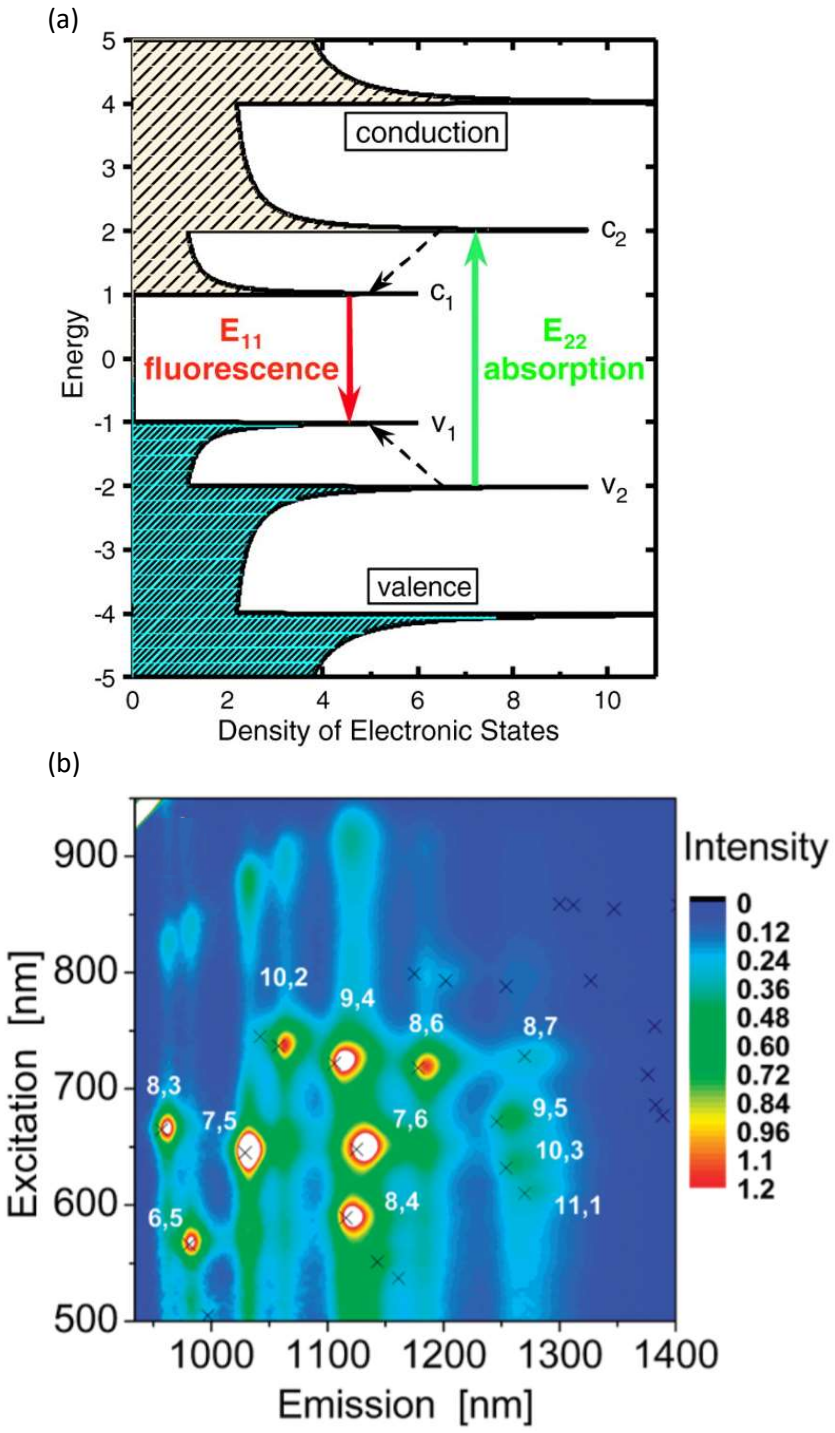

Figure 1-4: Fluorescent properties of SWNT. (a) Representational density of electronic states for a single nanotube complex. Solid arrows represent the optical excitation and emission transitions responsible for the fluorescence of interest; dashed arrows describe nonradiative relaxation of the electron in the conduction band and valence band prior to emission. Reprinted with permission from Science [8, 121]. (b) Optical Emission and excitation wavelengths of various SWNT chirality's. Reprinted with permission from Blum et al. [139]. Copyright (2011) American Chemical Society

1.3 Sensor Applications of Fluorescent Single Walled Carbon Nanotubes

1.3.1 Ex Vivo Applications

In many cases it is convenient to detect analytes of interest from biological samples, such as blood or cell culture supernatant. Fluorescent SWNT has been used extensively to detect a variety of analytes in this manner including genetic material, proteins, hormones, and key components of cell culture (Table 1-1).

Genetic materials that have been detected include hybridized DNA, single nucleotide polymorphisms (SNPs), and miRNA [2-4, 6]. The detection of DNA and miRNA hybridization using SWNT could be used for the detection of genetic material from pathogenic organisms in both humans and plants [140-142]. In fact, a SWNT sensor which detects human immunodeficiency virus (HIV) RNA has already been developed, which could help medical personnel rapidly identify HIV carriers before symptoms are detectable [3]. Meanwhile, SNPs, which are detected through incomplete hybridization events, have been linked to the formation of genetic disorders [2, 143], a proclivity to the development of disease [144], and a disparity in patient reaction to certain treatments [145]. Rapid SNP detection at the clinical level could help tailor treatment on a patient by patient basis. SWNT has also been extensively used to detect proteins like, avidin, the HIV-1 integrase protein, the RAP-1 protein and cardiac troponin through the use of binding domains which include aptamers, antibodies, and biotin [7, 8, 75, 76]. The detection of proteins in biological media can have prompt, low risk clinical applications, such as the rapid confirmation of acute myocardial infarction with the cardiac troponin

sensor [7]. SWNT sensors have also been employed to detect key hormones such as insulin, L-Thyroxine, and estradiol [77, 78]. The use of SWNT to detect hormones could have direct and immediate implications. For instance, the insulin sensor could be applied for rapid diabetic assessments, the L-throxine sensor could prove useful for monitoring hypothyroidism treatment, and estradiol detection could be used to monitor the treatment of certain breast and prostate cancers [146, 147].

Table 1-1: Published ex vivo applications of SWNT

Analyte Detected	**Detection Medium**	**Wrapping Employed**
HIV RNA [3]	Serum	$(GT)_{15}$-$(T)_{15}$
miRNA Hybridization [6]	Serum, Urine	$(GT)_{15}$-miRX
Single nucleotide polymorphisms [2]	Water	5'–TAGCTATGGAATTCCTCGTAGGCA – 3'
DNA hybridization [4]	Water	5'-TAG CTA TGG AAT TCC TCG TAG GCA-3'
Avidin [75]	Water	Dye ligand conjugates doped SDS micelles
human IgG, mouse IgM, rat IgG2a, and human IgD [74]	PBS	Chitosan/immunoglobulin-binding protein complex
Troponin T [7]	Serum	Chitosan/anti-troponin antibody complex
Insulin [77]	PBS, Serum	PEGylated lipid heteropolymer
L-Thyroxine [78]	PBS	Fmoc-Phe-PPEG8
Estradiol [78]	PBS	RITC-PEG-RITC
Riboflavin [78]	PBS	BA-PhO-Dex
Nitric Oxide [9]	PBS	$d(AT)_{15}$
Hydrogen Peroxide[133]	Saline	$d(GT)_{15}$
HIV1 integrase protein [8]	PBS	$(AT)_{11}$-HIV-1 aptamer
RAP-1 Protein [8]	PBS, Crude cell lysates	$(AT)_{11}$-RAP1 aptamer complex
Catecholamines (DA and NE) [84]	PBS, Striatal Brain tissue	$(GT)_6$
B-D-glucose [148]	TRIS buffer	Glucose oxidase
pH [149]	Water	SDBS micelle
Ag+ and cysteine [150]	HEPES buffer	FAM labeled 5'-CTC TCT CTC TCT CTC TCT CTC-FAM-3'
Co^{2+} Ca^{2+} Mg^{2+} [72]	PBS	$d(GT)_{15}$
Hg^{2+} [72]	PBS, Whole rooster blood, Chicken tissue	$d(GT)_{15}$
Doxorubicin [151]	Saline-sodium citrate buffer	$(GT)_{15}$

1.3.2 In Vitro Applications

As sensors, SWNT have been used for the detection of a wide range of intracellular molecules and analytes in various cell lines (Table 1-2). One of the more prominent examples of *in vitro* detection includes the detection of NO in A375, HUVEC and Raw 264.7 cells [69, 79], where it was demonstrated for the first time that the A375 melanoma cell line possess at least 1 source of NO production and 2 sinks [69]. SWNT have also been used to detect endosomal lipid accumulation in RAW 264.7 cells [1]. The ability to detect endosomal lipid flux could be critical to increasing our understanding of various diseases where an accumulation of lipids within the endosome has been observed, including liver disease, neurological disorders, and cancer [152-154]. SWNT have also been used for the detection of the HER2/neu receptor in BT-474 cells [155] and the detection of riboflavin in Raw 264.7 macrophage cells [78]. The detection of cell surface receptors like HER2/neu in conjunction with proteins like Riboflavin are important in the detection and study of breast cancer where the HER2/neu is often over expressed in conjunction with elevated levels of Riboflavin absorption [156, 157]. It is generally accepted that SWNT enter cells via an energy-dependent endocytic route where they are incorporated into the endosomal lumen of cytoplasmic vesicles [1, 138, 158, 159].

Table 1-2: Published intracellular in vivo applications

Analyte Detected	**Cell lines used**	**Wrapping Employed**
NO [69]	A375, HUVEC	$d(AT)_{15}$
NO [79]	Raw 264.7	DAP-DEX
H_2O_2 [133]	Murine NIH/3T3	$d(GT)_{15}$
Riboflavin [78]	Raw 264.7	BA-PhO-Dex
Lipids [1]	RAW 264.7, U2OS-SRA, primary monocytes, patient derived fibroblasts	$(GT)_6$
CD20 cell surface receptor [155]	Raji	PEG-Rituxan
HER2/neu [155]	BT-474, and MCF-7	PEG- Herceptin
ATP [81]	HeLa	PLPEG - luciferase
Hg^{2+} [72]	3T3 Fibroblasts	$d(GT)_{15}$
6 genotoxic elements [133]	Murine 3T3	$d(GT)_{15}$
Doxorubicin [151]	RAW 264.7 murine macrophage	$(GT)_{15}$

In some instances, it is more appropriate or desirable for the researcher to monitor extracellularly excreted proteins and cell signaling molecules while remaining in the *in vitro* environment (Table 1-3). SWNT has been used on several occasions to provide information about the extracellular secretions of cells. On one such occasion SWNT was used for the high resolution spatio-temporal detection of dopamine efflux from PC-12 cells [73]. The detection of neurotransmitters like dopamine have implications for advancing our understanding of neuronal function and the pathophysiology of its dysregulation. This method of detection has already been used to discover that dopamine efflux is greatest from the negative curvature regions of cellular protrusions rather than the commonly held belief that efflux is greatest at the tips of protrusions [73]. Moreover, SWNT has been shown capable of detecting RAP-1 protein secretions from *E. coli* and

the HIV-1 integrase protein excretion by HEK and yeast cells [8]. The detection of proteins from individual cells provides valuable information about transcription and translation rates. Using this method of detection, the authors were able to determine that non-dividing *E. coli* had a smaller protein secretion footprint and were slower to produce protein after induction. They were also able to detect RAP-1 protein released after cell lysis in *E. Coli* infected with T7 bacteriophages carrying the RAP1 gene, thus allowing for the visualization of individual cell lysing events and easy fluorescent tracking [8]. Additionally, SWNT has been used for the detection of H_2O_2 signaling from A431 and HUVEC cells [10, 71]. The detection of reactive oxygen species (ROS) and reactive nitrogen species (RNS) signaling molecules has remained difficult due to their high reactivity and short lifetimes. The ability to form a sensor array in close proximity to the cell promises an understanding of real time signaling dynamics which was not previously possible. Unfortunately, while monitoring extracellular secretions is often desirable, the current methods of SWNT deposition are not well characterized or well suited to vigorous cell culture applications, relying almost entirely on non-specific interactions, matrix immobilization, or electrostatic deposition. Matrix immobilization methods suffer from poor response times [10], while non-specific and electrostatic methods are subject to interference from other biomolecules [160, 161]. A more robust and well characterized method of SWNT deposition is necessary for continued research on extracellular signaling.

Table 1-3: Published intercellular in vivo applications

Analyte Detected	**Cell line**	**Wrapping**
Dopamine [73]	PC-12	$(GA)_{15}$
RAP-1 protein [8]	E. Coli	$(AT)_{11}$-RAP1 aptamer complex
HIV-1 Integrase protein [8]	Yeast, HEK293	$(AT)_{11}$-HIV-1 aptamer complex
H_2O_2 [10, 71]	A431, HUVEC	Collagen

1.3.3 In Vivo Applications

SWNT have also been used *in vivo,* although these instances are less frequent (Table 1-4). One such sensor that has been successfully employed *in vivo* is the NO sensing SWNT in SJL mice. This sensor was successfully employed to detect local levels of NO increase due to inflammation [5]. Another SWNT sensor that has been used in animal models is an LDL cholesterol sensor, which was used in C57BL/6 mice [80]. This sensor has already been used to demonstrate the prolonged negative effects of poor diet on mice suffering from nonalcoholic fatty liver disease even after returning to a healthy lifestyle.

Table 1-4: Published in vivo applications

Analyte Detected	**Animal Model**	**Wrapping employed**
NO [5]	SJL mice	PEG-$(AAAT)_7$
LDL Cholesterol [80]	C57BL/6 mice	5'-CTTC3TTC-3'
Doxorubicin [151]	NU/J (nude) mice	$(GT)_{15}$
Dopamine [162]	Drosophila embryos	GFP Binding Protein/d(GT)20 conjugate
Riboflavin [163]	Nine species of bony fish, sharks, eels, and turtles	$(AC)_{15}$

1.3.4 Single Walled Carbon Nanotube Biocompatibility

As a result of SWNT's potential application to the biomedical field, considerable effort has been spent determining the consequences of SWNT introduction on cell health. A number of studies have indicated that raw SWNT may negatively impact cell viability [164-166]. However, these results have been called into question by numerous additional publications specifically due to the interference of raw SWNT with common assays used to determine cell health [167-169]. To date raw SWNT has been shown to interact with many popular assays for measuring cell health, including MTT, WST-1, Alamar Blue, Neutral Red, and Commassie Blue, providing false indications of cell distress [167-169]. The interaction between SWNT and these reagents is not fully understood, but it is believed that hydrophobic regions of crucial signaling dyes and probes often aggregate around the raw single walled carbon nanotubes causing disruptions in their ability to accurately relay information about cell health. Studies which use indicator dyes and fluorophores in conjunction with raw SWNT should be taken with much skepticism. Studies which rely on morphological assessments of raw SWNT toxicity have found that

the addition of raw SWNT at low concentrations (25 mg/L) to cell culture media can cause changes indicative of apoptosis in HEK 293 cells including: an increase in membrane vesicles, nucleus condensation, fragmentation, and cell rounding [170]. At higher concentrations (400 mg/L) morphological characteristics of increased apoptosis continue in A549 cells, but necrosis also begins to take place [171].

However, the toxicity of raw SWNT has a limited impact when considering sensor applications since raw SWNT are unlikely to be used as fluorescent sensors for biologically relevant molecules, instead they are solubilized with wrappings (polymer or DNA) as previously discussed. Unfortunately, the issue of wrapped SWNT toxicity in cell culture becomes increasingly uncertain due to a lack of literature regarding the effects of wrapped SWNT on common assays of cell health. It is not understood if, like its unwrapped counterpart, hydrophobic interactions skew results of cell viability assays or if the presence of DNA/polymers is sufficient to prevent adsorption of indicators. Despite this fact, some assays have been performed which indicated that wrapped SWNT does not have an impact on the viability of HeLa and SiHa cells at concentrations of 0.1-2 mg/L after a 24 hour incubation period [172]. Wrapped SWNT was also found to not impact the viability of IMR 90 cells at concentrations of 20 mg/L or less after a 16 hour incubation period [173]. Finally, wrapped SWNT was found to have no effect on the proliferation and viability of RAW 264.7 macrophage cells when incubated at a concentration of 0.2 mg/L for 24 hours [1]. Moreover, shorter carbon nanotubes (< 500 nm), like those used in the preparation of SWNT sensors, are considered to be safer for use in cell culture [174]. Although the *in vitro* effects of wrapped SWNT remain ambiguous and controversial, fluorescent SWNT has been consistently shown to have

minimal or no impact on animal well-being and are generally expected to be expelled from the body via the biliary and renal pathways [175-179]. In a more recent study, DNA wrapped SWNT were implanted into mouse models for nearly one year with no signs of toxicity or SWNT degradation [5].

1.4 SWNT Complex Deposition

Carbon nanotube deposition to cell culture surfaces is critical for many SWNT applications including the high spatio-temporal imaging of cellular signaling and excretions [8, 10, 71, 73, 180], high-throughput screenings of biomolecules [74, 180], and comparative dynamic studies [181]. Unfortunately, current methods of SWNT deposition are often poorly described and documented. Keeping this in mind, the methods of SWNT deposition fall broadly into two categories: (1) matrix immobilization or (2) surface decoration through the use of electrostatic or non-specific interactions.

1.4.1 Matrix Immobilization

One popular method of SWNT immobilization is the use of thin films. Thin collagen and chitosan films have been used to immobilize a variety of polymer -SWNT sensor complexes including those responsible for sensing H_2O_2, human IgG, mouse IgM, rat IgG2a, human IgD SWNT, and a variety of proteins [10, 71, 74, 180]. This method of

immobilization has benefited from both its simplicity and its potential for extensive secondary modification. Initial deposition of SWNT is generally a simple process whereby SWNT is suspended and wrapped in the matrix material via sonication. The SWNT/matrix composite may then be applied to the surface of a substrate (generally glass) and cross linked to form a stable SWNT sensor array. The addition of the matrix network allows for subsequent derivatization of the network, which may improve, or be necessary for, sensor performance. In some cases, the matrix is used to limit the diffusion of shorter-lived analytes emanating from cells and thus increase specificity for longer-lived analytes of interest [71]. Unfortunately, this method of deposition necessarily slows the diffusion of analytes to the SWNT sensor as proteins and other signaling molecules must navigate the matrix network to reach SWNT, negatively impacting the sensors temporal resolution. This can lead to lengthy sensor acquisition times such as a recently developed SWNT-collagen array designed to detect H_2O_2 which required 14 minutes to sense 1 uM H_2O_2 [10]. Moreover, although subcellular spatial resolution can be achieved using this method, it still lags behind other methods of SWNT deposition. As a result of these limitations, matrix immobilized SWNT are generally used for the detection of biologically relevant molecules in less time sensitive situations such as protein microarrays or they have been replaced by surface decoration methods [180].

1.4.2 Surface Decoration

In cases where high spatial and temporal resolution are required, such as the detection of cellular signaling molecules, surface decoration methods have been used with success to detect signaling molecules and proteins like NO, the RAP-1 protein, the HIV-1 integrase protein, dopamine, norepinephrine, and serotonin [8, 9, 73, 83, 84]. The most popular method of surface deposition is to use the electrostatic interactions between 3-aminopropyltriethoxysilane (APTES) and DNA-SWNT complexes [8, 9, 73, 84, 181]. In this case APTES solution, generally consisting of APTES (1%) in an anhydrous liquid (Ethanol), is applied to a glass surface where it forms a covalent bond with the surface via a condensation reaction [182]. The positively charged aminopropyl head can then undergo an electrostatic interaction with the negatively charged DNA backbone of a DNA-SWNT complex, thus immobilizing SWNT on the surface. In at least one case, neutravidin was used to form a non-specific bond with DNA-SWNT complexes to elicit SWNT deposition. In this case a mixture of PEG: Biotin-PEG was allowed to non-specifically adhere to a glass substrate followed by addition of neutravidin, which bound to the Biotin-PEG. SWNT was then added and deposition achieved by the non-specific interaction of SWNT with neutravidin [8]. Another approach to SWNT deposition utilizes the deposition of biotinylated BSA followed by neutravidin, and then biotinylated SWNT to generate a SWNT functionalized surface [133]. Unfortunately, this method was not well characterized and still relied upon the non-specific adsorption of biotinylated BSA to a glass surface to allow for neutravidin binding. Recently, a new method of SWNT deposition was attempted based on a covalent linkage of a chitosan wrapped

SWNT to a glass substrate derivatized with N-hydroxysuccinimide esters (NHS) [74]. The amine groups from the chitosan wrapping reacted with the NHS groups to form a covalent linkage. Unfortunately, this new method was not characterized due to a perceived decrease in the quality of the fluorescent distribution compared with electrostatic mechanisms [74].

1.5 Nitric Oxide

Until the late 1980's NO was best known for its formation in the exhaust of combustion engines and its subsequent participation in the formation of acid rain [183]. It came as no small surprise to the scientific community when, in 1987 it was discovered that NO was synonymous with endothelium-derived relaxing factor (EDRF), a factor which is critical to cardiovascular health. The discovery not only garnered, Robert F. Furchgott, Ferid Murad, and Louis J. Ignarro the Nobel Prize for Medicine or Physiology in 1998, but also prompted a new wave of NO study from a biological perspective, which has continued throughout the turn of the century [184]. After more than 30 years of research into NO's role in physiology, NO has been found to serve many functions which extend well beyond the cardiovascular system. As with most areas of physiology, following the discovery of NO's role in a biological system are subsequent findings about the role of NO's dysregulation in pathophysiological developments.

1.5.1 Nitric Oxide in Physiology

Although NO became famous for its role as the signaling molecule responsible for endothelial relaxation [185], it has since been discovered the NO plays an important role in many biological systems including the gastrointestinal tract, central nervous system, immune system, and renal system. In the gastrointestinal track, NO contributes to mucosal integrity through the inhibition of gastric acid release and the stimulation of mucosal and bicarbonate secretions [186-190]. In the central nervous system, NO acts as a neurotransmitter and plays a role in processing feelings of pain, appetite, and the sleep-wake cycle [17, 191-194]. NO may also act as a neuroprotective or degradative agent depending on its concentration in tissue [17, 195-198]. Within the immune system NO has been shown to have significant anti-microbial properties [199-201]. NO also serves additional functions within the cardiovascular system where it acts to mediate platelet aggregation and leukocyte adhesion (Figure 1-5).

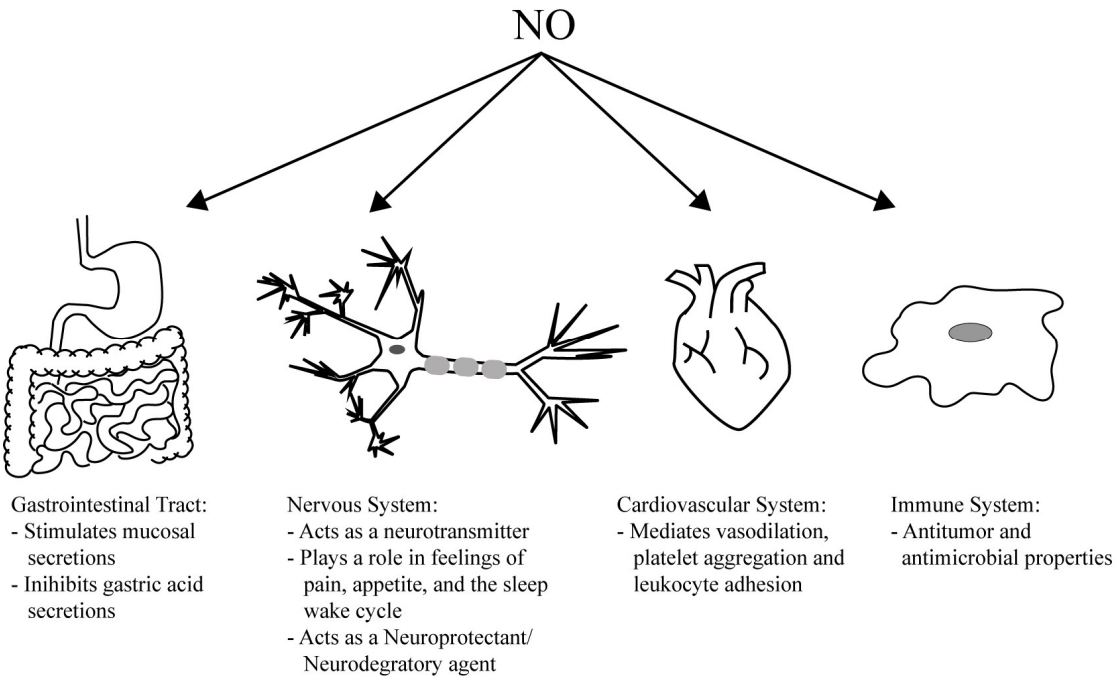

Figure 1-5: Roles of NO in physiology. NO plays a diverse role in numerous systems including the gastrointestinal tract, the nervous system, the cardiovascular system, and the immune system.

NO is generated by three isoforms of nitric oxide synthase (NOS): endothelial NOS (eNOS), neuronal NOS (nNOS), and inducible NOS (iNOS). Both eNOS and nNOS were named for the locations in which they were discovered and both isoforms are constitutively expressed, leading some researchers to refer to eNOS and nNOS collectively as constitutive NOS (cNOS). As the name suggests iNOS was named not for the location in which it was discovered, but for its presence in mammalian cells only after an immunological or stress stimuli occurs [202]. Functioning as a dimer, all three isoforms convert L-arginine, molecular oxygen, and NADPH into NO, NADP, and L-citrulline [203, 204] (Figure 1-3). Additional co-factors necessary for proper enzymatic function in the reductase domain include flavin-mononucleotide (FMN) and flavin adenine dinucleotide (FAD). Co-factors necessary for proper function in the oxygenase

domain include heme, zinc, tetrahydrobiopterin (BH_4) and calmodulin (CaM) [203]. While eNOS and nNOS are dependent upon intracellular calcium for proper CaM binding, iNOS, instead, produces NO continuously, and at much higher concentrations, when all cofactors are present [203].

In addition to its roles in normal cellular function, NO dysregulation has also been implicated in a host of pathophysiology's including cardiovascular diseases like hypercholesterolemia, atherosclerosis, diabetic angiopathy, hypertension, and cerebrovascular strokes[36-44] ; neurological disorders such as Alzheimer's and Parkinson's disease [32-35]; and inflammatory diseases like arthritis, Crohn's disease, and asthma [25-30]. Of particular interest is NO's role in carcinogenesis, where it has been found to have both pro and anti-tumor effects that appear to be highly dependent upon the spatio-temporal distribution of NO [19-24].

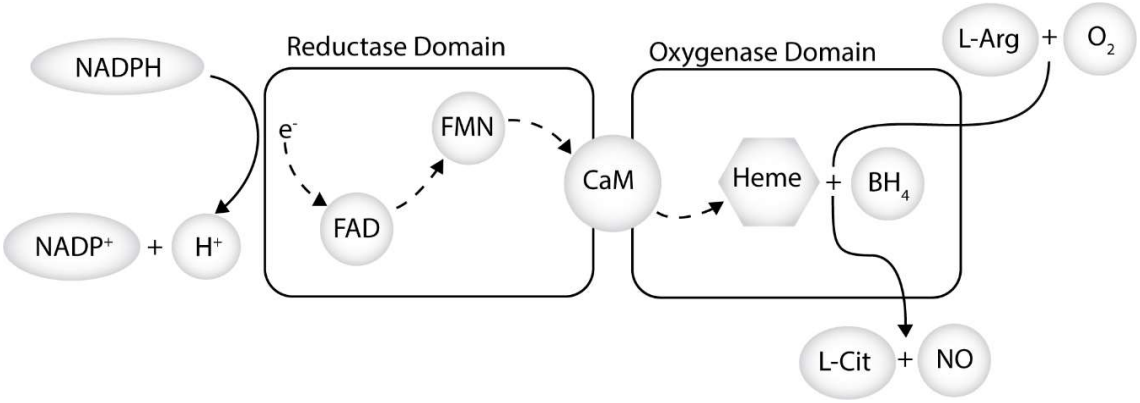

Figure 1-6: Production of NO from NOS. This schematic demonstrates the flow of electrons from NAPH through the NOS enzyme to the Heme of the oxygenase domain where L-Arg and O_2 are used as substrates to form L-Cit and NO. Note that the NOS enzyme shown here is displayed as a monomer for simplicity when NOS normally functions as a dimer. Created from material presented in Zhou et al. [205].

1.5.2 NO Measurement Techniques

The detection of NO has remained difficult due to its reportedly short half-life of less than 1 second in biological media [85-88, 206, 207]. Despite this fact, several assays are commonly used to determine NO concentration in biological systems besides SWNT. These methods will be discussed briefly below.

----------*Griess Assay*----------

The Griess assay is one of the most popular methods of approximating NO concentration in biological media. NO is rapidly converted into the relatively stable molecules of nitrite and nitrate in the presence of oxyhemoglobin and oxygen respectively, making them attractive targets for approximating NO concentration in biological settings [208, 209]. The Griess assay makes use of favorable interactions that can occur between a sulfanilamide and N-1-napthylethylenediamine dihydrochloride (NED). The addition of nitrite to these compounds causes their linkage and subsequent formation of an azo compound, which produces an observable absorbance shift. The concentration of nitrite is calculated using the absorbance shift and used as an indicator for NO concentration. The Griess assay benefits from its simplicity and commercially available kits, but suffers from indirect quantification of NO, a lack of spatial and temporal resolution, and inaccuracies from animal intake of nitrites/nitrates in food [210].

----------*NOS Activity*----------

While the Griess assay is concerned with measuring the downstream products of NO degradation, it is also possible to measure upstream components of NO production such as NOS activity. As explained previously, NOS requires L-arginine, NADPH, and oxygen as substrates to generate NO, NADP, and L-citrulline. In order to determine NOS activity, it is common to use radio labeled ^{3}H L-arginine and measure its conversion into ^{3}H L-citrulline. The remaining ^{3}H L-arginine can then be removed using a resin and the radioactivity of the ^{3}H L-citrulline sample measured using liquid scintillation counting. The radioactivity is considered proportional to NOS activity [211, 212]. Like the Griess assay this method of NO detection suffers from a lack of spatial and temporal resolution and requires the use of radiolabels, which many labs are not equipped to handle. Moreover, the use of this assay *in vivo* is generally not practical as it requires careful control of L-Arginine supplies [213].

----------*Fluorescent Detection*----------

One class of sensors which have shown the potential to detect spatial distributions of NO are fluorescent probes. Many fluorescent detection methods rely on *o*-diamino aromatic molecules, like the popular 4,5-diaminofluorescein (DAF-2). DAF-2 remains non-fluorescent until exposure to NO's autooxidation product N_2O_3 where it forms a fluorescent DAF-2 triazole (DAF-2T) [214]. Drawbacks of this assay include indirect measurement of NO, false identification of NO upon interaction with dehydroascorbic

acid (DHA) and ascorbic acid (AA), which often co-localize with NO, and sensitivity to pH [215-217].

Another commonly used class of fluorescent probes are those based on transition metal binding. It has long been known that NO can bind to transition metal complexes and in many cases, this is how NO signal transduction actually takes place[218]. Transition metal fluorescent probes aim to take advantage of this binding by using metal complexes containing cobalt (II), iron (II), ruthenium (II), dirhodium (II), or copper (II) which are bound to a fluorescent molecule [219]. When bound, the fluorescent molecule shows little or no fluorescence. After NO binding, the fluorescent molecule is displaced and fluorescence increases [220, 221]. Unfortunately, while these probes have the potential to provide high spatial and temporal resolution, many probes based on transition metals suffer from water insolubility, limiting their applications to biological systems [222]..

Quantum dots (QDs) have also shown promise in the detection of NO. To date both fluorescent turn “on” and turn “off” sensors have been developed using quantum dot cores [223, 224]. The turn off variety of QD sensors relies on a triethanolamine – CdSe – QD complex for the detection of NO. Normally, this complex’s fluorescence is increased in the presence of oxygen due to its ability to passivate surface defects [225, 226]. Because NO readily reacts with oxygen, it decreases the amount of oxygen present at the QD core and decreases fluorescent intensity. Additional evidence suggests that the adsorption of NO to the triethanolamine – CdSe – QD complex may also decrease fluorescence intensity [224]. This particular QD sensor suffers from a lack of specificity, a requirement of O_2 to function, and a mechanism that is not fully understood [227]. The

turn on variant of QD NO sensors relies on a tris(N-(dithiocarboxy)sarcosine)iron(III) ($[Fe(DTCS)_3]^{3-}$) complex being grafted to a CdSe-ZnS QD core. This QD sensor normally displays very little fluorescence due to charge transfer from the QD core to $[Fe(DTCS)_3]^{3-}$ complexes. However, upon exposure to NO, some or all of the DTCS is removed and replaced by NO, allowing for fluorescence to increase [223]. This QD sensor has excellent specificity and its mechanism is much better understood. Unfortunately, QDs continue to suffer from the fact that they are single use probes and thus lack the high temporal resolution desired by many researchers [227].

----------*Electron Paramagnetic Resonance Spectroscopy* ----------

Electron paramagnetic resonance spectroscopy (EPR) is a technique used to detect only paramagnetic molecules, that is molecules with one or more unpaired electrons, such as NO. Electrons can be thought of as spinning charges and as a result, they generate their own magnetic fields (dipole). Because electrons generate their own magnetic fields, they can be aligned by subjecting them to an external magnetic field. As a result of their quantum behavior, electrons can be considered to occupy only two states within the external magnetic field, aligned or not-aligned. Conceivably, a certain amount of energy could be imparted to the electrons via an X-ray source which would cause them to "flip" to a non-aligned position. At this point the electrons in the sample will be absorbing the energy provided by the X-ray in order to maintain their unfavorable position. If we record this position, we can generate an absorbance spectrum (or EPR spectrum). In reality it is the X-ray that is held constant while the magnetic field intensity is swept from high to low. The process is governed by the following equation [228]:

$$hv = g\beta B$$

$h = plank\ constant$
$v = frequency\ of\ X - ray$
$g = dimensionless\ constant\ charachteristic\ of\ the\ sample$
$\beta = Bohr\ Magnatron\ constant$
$B = External\ magnetic\ field$

When the equation is equal the sample absorbs energy and a peak is generated [229]. In its simplest form, a single electron, only a single peak would be generated, however the absorbance spectrum is also influenced by the presence of paramagnetic molecules close to the electron of interest (e.g. protons or nitrogen) which leads to an increase in the number, and complexity of, the generated peaks. The EPR spectra can be used to fingerprint molecules that contain unpaired electrons. NO has been observed in its gaseous phase using this technique [230], but is considered extremely difficult to detect in the liquid phase [229]. Thus, NO must be "spin trapped" or incorporated into another more stable and easily detectable molecule for observation via EPR. Common spin traps include nitroxides, cheletropics, nitronyl nitroxides, and the iron centers of heme-proteins [211, 231-238]. Unfortunately, the spin traps listed suffer from low sensitivity, a lack of specificity, and instability, making EPR difficult to perform *in vitro* or *in vivo* [211, 234, 235, 239].

----------*Chemiluminescent Probes*----------

An additional class of NO detectors takes advantage of the reaction between NO and soluble guanylyl cyclase (sGC), its natural target [240]. Upon NO binding, sGC

activity is increased nearly 100-fold, resulting in the rapid conversion of GTP to cGMP and pyrophosphate (PP_i). PP_i is then converted to ATP by ATP sulfurylase, which causes light emission from a luciferase-luciferin complex [241, 242]. Advantages of this method of NO detection include a large (200X) increase in fluorescence intensity following activation and the ability to detect NO at low concentrations [241, 242]. However, in order for this system to reach maximum sensitivity all NO should be bound to sGC meaning that additional sGC needs to be added to cell culture to achieve, which may prove cost prohibitive to researchers [242]. Furthermore, because this system requires ATP, NO cannot be accurately determined in cells which effuse ATP [242].

Unfortunately, current methods of NO detection suffer in one form or another from poor spatial or temporal resolution, poor specificity, indirect quantification, or poor outlooks for *in vitro* and *in vivo* biocompatibility. As previously mentioned, a new group of NO sensors based on DNA-SWNT complexes have shown the potential to overcome these problems by providing high quality spatial and temporal information about NO *in vitro* and *in vivo* by detecting NO directly with a high degree of specificity [5, 9, 69].

1.6 Thesis Objectives

Fluorescent DNA-SWNT complexes have a range of advantageous properties as sensors, but many potential applications are reliant on the efficient deposition of SWNT for the detection of extracellular analytes. Currently available SWNT deposition procedures are poorly characterized and rely almost entirely on electrostatic or non-

specific strategies. The use of the avidin-biotin bond to enhance SWNT deposition shows the potential to overcome the shortcomings of the previous methods of SWNT deposition. The goals of this thesis were to develop an improved deposition method by: (1) determining if biotin activity can be imparted to SWNT via biotinylation of the DNA wrapping, (2) determining if biotinylation damages SWNT's spectral properties, (3) fully characterizing a new method for depositing SWNT to a glass surface using an avidin-biotin bond where avidin is covalently bound to the glass substrate, (4) fully characterizing the current standard for SWNT deposition which relies on electrostatic interactions for SWNT deposition and serves as the current standard, (5) determining if the avidin-biotin bond can enhance deposition rates without harming some of those properties which are already enjoyed by previous methods of SWNT deposition. Chapter two will detail the results of this investigation demonstrating the significant increase in DNA-SWNT complex deposition using the avidin-biotin bond. Chapter three will then outline future studies for the continuation of SWNT deposition enhancement.

CHAPTER 2

Improving SWNT Deposition Efficiency

2.1 Introduction

The detection and study of extracellular products has been under intensive study for the past several decades due to the fundamental role signaling molecules play in coordinated biological processes [243-246]. There are currently many methods which allow for the temporal study of extracellular products, but very few which allow for the simultaneous study of their spatial distribution [247-252]. Recently, a new group of sensors based on DNA wrapped fluorescent single walled carbon nanotubes (SWNT) have shown the potential to provide high quality spatial and temporal information regarding a wide range of cellular signaling molecules, proteins, and analytes including nitric oxide (NO), hydrogen peroxide (H2O2), glucose, dopamine, norepinephrine, serotonin, lipids, oligonucleotides, and the RAP-1/HIV-1 integrase proteins [1, 6, 8, 9, 70, 71, 73, 80, 83, 84]. In addition to their ability to sense key signaling molecules, SWNT offer several advantages over other sensors including a fluorescent signal in the near infrared tissue transparency window, no blinking or photobleaching, and, as a result of its small size, the potential to create high density sensor arrays [121, 122, 131, 148, 253-257].

Depositing SWNT on cell culture substrates is a critical step in the formation of sensor arrays, however current methods for the deposition of DNA-SWNT complexes are limited almost entirely to matrix immobilization techniques, electrostatic interactions,

and non-specific interactions which are subject to one or more shortcomings [8-10, 73, 83, 84]. The most straightforward method of SWNT deposition is matrix immobilization. In this case the SWNT is suspended in a polymer (e.g. collagen) and cross-linked to form a cell culture surface [10, 71]. Unfortunately, this method of SWNT preparation suffers from a long acquisition time (14 minutes to detect 1 uM H_2O_2) [71]. Throughout the acquisition time a laser or other light source must be used excite the SWNT within the matrix [71]. Prolonged exposure of cell cultures to laser light in conjunction with their removal from the incubator can have unintended effects on cell culture [258-260]. Moreover, because analytes must navigate the matrix of thin films to reach SWNT, only the most stable analytes can be detected, excluding the applicability of this platform to shorter lived analytes such as NO [71].

In light of the shortcomings of matrix immobilization techniques several surface decoration methods have been developed with the goal of decreasing acquisition time and improving sensor responsiveness to all analytes. The most common and current standard method of SWNT decoration relies on the use of an aminopropyl silane which is bound to a glass substrate [8, 9, 73, 261]. The partially negative DNA strand that wraps the SWNT sensor (i.e. the DNA backbone) is allowed to interact with the partially positive aminopropyl derivatized surface, generating a SWNT functionalized surface through electrostatic interactions. A less common method which has been employed relies upon non-specific interactions between SWNT and avidin isoforms (neutravidin and streptavidin), however this method has yet to employ a covalently bound avidin molecule and instead relies upon non-specific interactions between the glass surface and the avidin protein [8, 261]. A final approach to SWNT deposition utilizes biotinylated BSA

followed by neutravidin, followed by biotinylated SWNT to generate a SWNT functionalized surface [133]. Unfortunately, in this paper the activity of biotin following its addition to SWNT was not confirmed and relied upon non-specific interactions between BSA and the underlying glass substrate [133]. All of the surface decoration methods listed here rely upon non-specific or electrostatic interactions at some level of their design. Non-specific and electrostatic interactions are notoriously unstable, lack reproducibility, and are subject to interference from other biomolecules, making them undesirable for long term cell culture applications [161, 262]. These methods have also suffered from low quantities of SWNT at the surface requiring the use of high power magnification (50X or greater) and high laser power (450 mW at the source)[8, 9]. The use of high power magnification is problematic for the study of large scale signaling events *in vitro,* while the high laser power may have unintended effects on the cells of interest [258-260].

A logical next step for the development of SWNT functionalized surfaces would be to eliminate electrostatic and non-specific deposition methods from surface functionalization schemes and instead rely completely on covalent bonds or bioaffinity interactions. Depositing SWNT in this manner eliminates reliance on unstable deposition methods, while maintaining the high reactivity of current decoration methods. Moreover, this process has the potential to increase the quantity of SWNT at the surface, thus increasing the fluorescence and allowing lower power objectives to be used at a lower microscope power. One way to achieve a high concentration of SWNT deposition would be to covalently bind avidin to the cell culture surface and enhance SWNT attachment through the use of well-characterized biotinylated-SWNT.

Herein we utilize a new method for the deposition of SWNT sensors based upon the avidin – biotin interaction. We take advantage of the simple addition of biotin to DNA oligo tails and utilize an epoxy silane linker to bind avidin covalently to the underlying glass substrate. We compare this new method of SWNT deposition with the current standard (APTES). Our results demonstrate the successful addition of biotin to SWNT sensors without altering function, the covalent linkage of avidin to a glass substrate, and an increase in the quantity of SWNT at the surface without damaging SWNT distribution or response time. We chose to use the 6,5 $d(AT)_{15}$ NO sensing SWNT as a proof of concept sensor for this platform due to its relative simplicity compared to some of the more complex DNA-SWNT sensors [6, 8] and its widespread application possibilities, including analysis of vasodilation, immune function, and neurological signaling, which are dependent upon NO spatial concentrations [263-270].

2.1.1 Fabrication of SWNT Derivatized Substrates

Figure 2-1a shows the fabrication process for the production of SWNT derivatized surfaces utilizing an avidin substrate. Slides were derivatized with SWNT via a 4-step process: (1) Slides were immersed in piranha solution to generate hydroxyl groups. (2) Slides were transferred to a 3-glycidoxypropyltrimethoxysilane (3-GPTMS) solution followed by oven curing to generate a 3-GPTMS network on the surface. (3) Avidin was applied to the surface and the primary amines allowed to interact with the epoxide rings of 3-GPTMS generating a covalent bond between 3-GPTMS and avidin.

(4) Non-biotinylated-SWNT (NB-SWNT) is applied to the surface where the negatively charged DNA backbone interacts with the positively charged avidin protein OR biotinylated – SWNT (B-SWNT) is applied to the surface where avidin-biotin binding may take place in conjunction with any non-specific interactions. Figure 2-1b shows the fabrication process for the production of SWNT derivatized surfaces utilizing a 3-aminopropyltriethoxysilane (APTES) substrate. Slides were derivatized via a 3-step process: (1) Slides were immersed in piranha solution to generate hydroxyl groups. (2) Slides were transferred to an APTES solution followed by oven curing to generate an APTES network on the surface. (3) SWNT is applied to the surface where the partially negatively charged DNA backbone interacts electrostatically with the aminopropyl head of APTES.

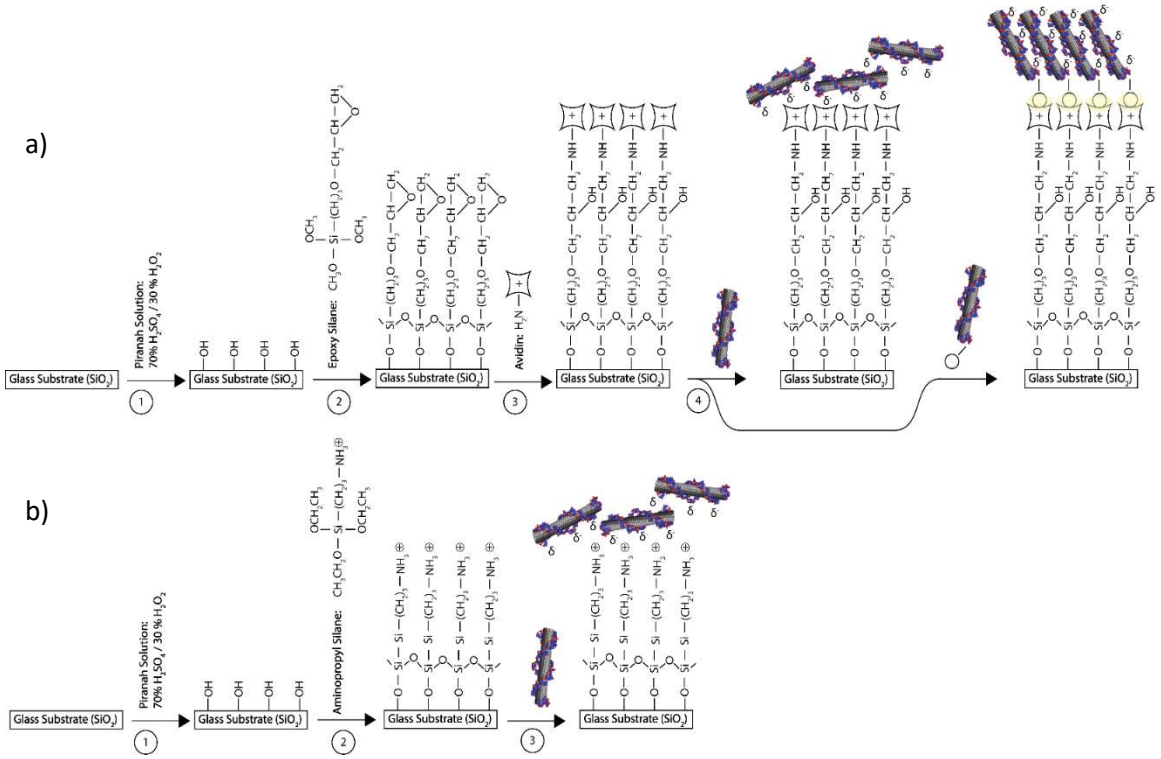

Figure 2-1: Fabrication of SWNT derivatized substrates. a) Derivatization of the glass surface with avidin follows a three step process: (1) glass slides are treated with piranha solution to generate hydroxyl groups at the surface (2) 3-GPTMS is allowed to react with the exposed hydroxyl groups and bind to the surface (3) exposed amine groups on avidin react with the epoxide rings of GPTMS, tethering avidin to the surface. SWNT may be deposited on avidin via non-specific interactions such as electrostatic interaction between the DNA backbone and the positively charged avidin, or biotinylated SWNT may be used to enhance binding through the specific avidin-biotin interaction. (b) APTES is functionalized similarly to 3-GPTMS: (1) slides are treated with piranha solution (2) slides are allowed to react with APTES forming a covalent bond. SWNT can then be applied and allowed to interact electrostatically.

2.2 Methods

2.2.1 Dispersion of 6,5 SWNT via DNA Oligos

SWNT was dispersed via DNA oligos similar to methods previously described [9, 136]. Briefly, CoMoCat 6,5 SWNT (Sigma) were wrapped with either $d(AT)_{15}$ ssDNA alone or a 1:1 volumetric ratio of 5'-biotinylated $d(AT)_{15}$ to $d(AT)_{15}$ ssDNA (Integrated

DNA Technologies). Wrapping procedures were identical regardless of the presence or absence of biotinylated DNA. SWNT and ssDNA were combined in a 2:1 mass ratio in nanopure water. The SWNT, DNA, and water mixture was then bath sonicated for 10 minutes followed by ultrasonic tip sonication (QSonica Q125 Sonicator) with a 3mm probe tip in two 20 min intervals at approximately 4 watts, the SWNT suspension was then centrifuged for two 90 min sessions at 16100 RCF (Beckman Coulter Microfuge 16). The top 80% of the SWNT supernatant was retrieved after each centrifugation and the pellet was discarded to remove unwrapped SWNT bundles. SWNT concentration was obtained via UV-Vis spectroscopy (Beckman Coulter, DU 730) and diluted to appropriate concentrations [9]. SWNT was stored at 4 C for up to 1 month.

2.2.2 Generation of Avidin – Biotin – SWNT Derivatized Surfaces

Avidin derivatized slides were generated as previously described with minor alterations [15, 271]. Briefly, low-iron soda lime glass microscope slides (Corning) were treated with a 70% sulfuric acid (Sigma)/30% hydrogen peroxide solution (Fisher) for 16 hours. Slides were then washed with copious amounts of nanopure water, rinsed 3 times in ethanol and dried under an argon stream before being transferred to a solution consisting of 95% ethanol, 16mM acetic acid (Honeywell), and 1% (3-Glycidopropyl)trimethoxysilane (Sigma) for 24 hours. Slides were then rinsed with ethanol 3 times and cured in a 150 C oven for 3 hours. Slides were allowed to return to room temperature, rinsed with ethanol 3 times, and allowed to dry. 60 uL of 1 mg/mL

avidin (Sigma) in 10mM $NaHCO_3$ was then added to the surface of the slide, covered with a plastic coverslip (22 mm x 22 mm), and allowed to incubate overnight at 37 C. Coverslips were removed and slides rinsed with copious amounts of nanopure water. Slides were then blown dry under an argon stream. 60 uL of a 2mM aspartic acid in 0.5M $NaHCO_3$ buffer was added to the surface and covered with a coverslip for 30 minutes to quench any remaining epoxide groups. Coverslips were removed and slides washed with copious amounts of nanopure water. Slides were blown dry with an argon stream. 60 uL biotinylated or non-biotinylated SWNT was then added to the surface at the desired concentration and allowed to incubate for 24 hours at 37 C. Coverslips were removed and slides were washed with copious amounts of nanopure water. Slides were stored in individual holders and used after a 2-hour equilibrium period.

2.2.3 Generating ATPES Derivatized Surfaces

APTES slides were generated similarly to avidin derivatized slides. Briefly, low iron soda lime glass microscope slides were treated with a 70% sulfuric acid/30% hydrogen peroxide solution for 16 hours. Slides where washed with copious amounts of nanopure water, rinsed 3 times in ethanol and dried under argon before being transferred to a solution consisting of 95% ethanol, 16mM acetic acid, and 1% (3-Aminopropyl)triethoxysilane for 24 hours. Slides were then rinsed with ethanol 3 times and cured at 150 C for 3 hours. Following cooling, slides were rinsed 3 times with ethanol and allowed to dry. 60 uL of SWNT at the desired concentration was then added

and covered by a coverslip. Slides were allowed to incubate with SWNT for 24 hours at 37 C. Following incubation, slides were washed with copious amounts of nanopure water and stored in individual holders. Slides were used after a 2-hour equilibrium period.

2.2.3 X-ray Photoelectron Spectroscopy Measurements

X-ray photoelectron spectroscopy (XPS) measurements were taken using the K-alpha^{+} XPS/UPS system (Thermo) with an AI Kα micro-focused monochromator X-ray source. Backgrounds were removed, atomic percent calculated, and peaks identified using Avantage software.

2.2.4 Contact Angle Measurements

Static contact angle images were captured using an Attension Theta Optical Tensiometer (Biolin Scientific) and analyzed using the OneAttension Software. ddH_2O drops were used. A 1 uL drop size was used in all cases. Droplets were analyzed for 5 seconds and the contact angle achieved at 3 seconds used to allow for settling effects.

2.2.5 HABA Assay

Biotinylation of DNA oligos was determined with a 4′-hydroxyazobenzene-2-carboxylic acid (HABA) assay (Thermo) using the protocol provided by Thermo Scientific. Briefly, HABA dye binds to avidin and produces an absorbance spike at 500 nm. Once biotin is introduced it displaces HABA from avidins active sites and reduces the absorbance at 500 nm. The change in absorbance can be used to calculate the concentration of active biotin within the sample of interest. Furthermore, when the molecular weight of the sample is known, as is this case (AT_{15} MW = 9199.1$\frac{g}{mol}$), it is possible to calculate the average number of active biotin per DNA [272] All measurements were recorded using the cuvette format on a UV-Vis spectrometer (Beckman Coulter DU 730).

2.2.6 Horseradish Peroxidase Assay

NO concentration of deoxygenated ddH_2O was quantified using a Horseradish peroxidase (HRP) assay as previously described [273]. Briefly, NO was added to HRP (Thermo) for a final concentration of 1.36 uM HRP. The absorbance was collected from 300 – 650 nm using a UV-Vis spectrometer (Beckman Coulter DU 730) and the underlying HRP spectra removed. The second order derivative was determined using MATLAB. Derivative spectra were smoothed using a Savitsky-Golay algorithm (order =

3, frame length = 51). The NO concentration was then calculated using the difference between the peak at 210 nm and the valley at 240 nm.

2.2.7 Fluorescent Measurements and Microscopy

Measurements of SWNT fluorescence intensity and spectrum were determined with a custom built near infrared (nIR) microscope (Photon). The setup is similar to one previously published [274]. Briefly, SWNT samples were excited by a 561 nm laser, the resulting emission was then passed through a volume Bragg grating (VBG) twice to reduce bandwidth and specify wavelength. Sample intensity was recorded across wavelengths to generate a hyperspectral cube. The cube was processed with PHySpec (Photon) software to generate images at the desired wavelengths. Pixel-by-pixel intensity information was captured using an InGaAs camera (Xenics, Xeva-1.7-320 TE3).

When only 990 nm fluorescent intensity was desired a 990 nm band pass filter (Thor Labs) was used rather than the VBG system.

2.3 Results and Discussion

2.3.1 Generating Biotinylated SWNT

Raw 6,5 SWNT was wrapped with a 1:1 volumetric ratio of biotinylated- $d(AT)_{15}$ DNA to $d(AT)_{15}$ by sonication. Following sonication, remaining raw SWNT was removed via centrifugation. In order to ensure biotinylated -$d(AT)_{15}$ was not only present on the SWNT, but also that the biotin was available for avidin biding, a 4'-hydroxyazobenzene-2-carboxylic acid (HABA) assay was conducted. Using the HABA assay we tested the availability of biotin from the following conditions: (a) stock DNA (b) sonicated DNA (c) sonicated and centrifuged DNA and (d) sonicated and centrifuged DNA with SWNT (Table 2-1). Intermediate DNA stages without SWNT were included to determine if any losses in biotin activity could be attributed to sonication or centrifugation alone (without SWNT). The intermediate DNA samples showed no substantial decrease in biotin activity, indicating that sonication or centrifugation in the manner necessary for SWNT production are not inherently damaging to biotinylated DNA. Wrapped SWNT maintained biotin availability (0.2025 biotin/DNA), with a slight, decrease in biotin availability compared to stock DNA samples (0.3623 biotin/DNA). Loss of biotin activity could be a result of non-specific interactions between the biotin molecule and the SWNT or due to physical disturbances only achieved when SWNT is present, such as increased temperature during sonication or centrifugation. Changes to SWNT wrapping procedures may be able to alleviate some of these issues. The remaining active biotin can be used to calculate an average number of available biotin per SWNT. Using the approximation that SWNT prepared in this manner are ~ 100 nm long and the

number of DNA wrappings per 600 nm is ~ 187.5 we can determine that there are 31.25 DNA strands per SWNT [122, 275, 276]. Multiplying the number of strands per SWNT by the number of biotin per DNA yields an average of ~6 biotin per SWNT.

Table 2-1: HABA assay results. The concentration of available biotin (mmol biotin/ mL) reaction mixture for stock DNA, sonicated DNA, sonicated and centrifuged DNA, and DNA wrapped SWNT was calculated using the Δ absorbance at 500 nm and the HABA assay. Using the molecular weight of the biotinylated molecule, in this case $(AT)_{15}$ DNA (9199.1 g/mol), the number of biotin/DNA was calculated. DNA Wrapped SWNT maintained biotin availability following sonication (0.2025 biotin/DNA). Using an average number of 31.25 $(AT)_{15}$ DNA strands per SWNT the number of available biotin/SWNT was calculated to be ~ 6.

DNA State	Δ absorbance	mmol biotin/ mL reaction mixture	Available biotin/ DNA
(a) Stock DNA	0.2678	7.876E-06	0.3623
(b) Sonicated DNA	0.2560	7.529E-06	0.3463
(c) Sonicated & Centrifuged DNA	0.2521	7.415E-06	0.3410
(d) Wrapped SWNT	0.0150	4.402E-06	0.2025

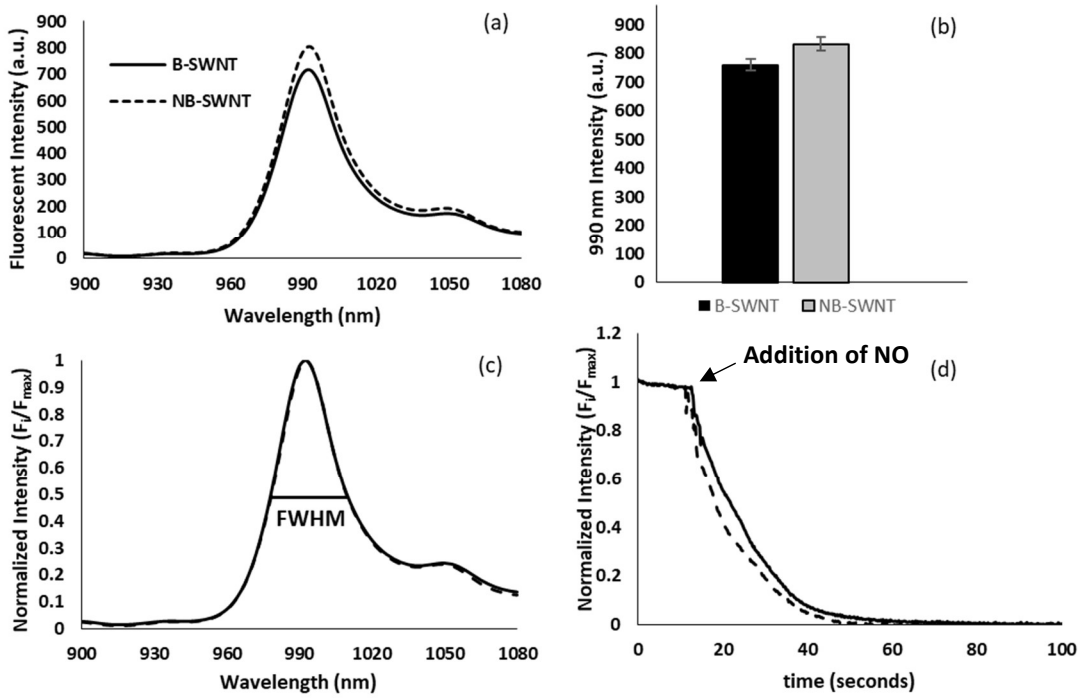

Figure 2-2: Behavioral properties of biotinylated SWNT (A) Fluorescence emission spectra for 10 mg/L B-SWNT (dashed) and NB-SWNT (solid) at 10 mg/L. (B) Isolated 990 intensity values for B-SWNT and NB-SWNT demonstrate negligible differences (C) Normalized fluorescent spectra demonstrate identical full width half max values (FWHM) (D) Fluorescence quenching curves in response to identical concentrations of NO demonstrate that biotinylation has a negligible effect on SWNT quenching response.

Following wrapping, measurements were conducted to ensure that the sensors maintained their characteristic peak and intensity structure. B-SWNT and NB-SWNT were diluted to a concentration of 10 mg/L and intensity spectrums collected using hyperspectral microscopy (n=4) (Figure 2-2a). Isolation of the 990 nm fluorescence demonstrated a negligible difference between intensity values of B-SWNT and NB-SWNT (Figure 2-2b). Comparison of the normalized intensity spectra indicated that biotinylation had no effect on the FWHM of the SWNT emission peak (Figure 2-2c).

Next, the quenching capacity of B-SWNT was tested and compared with that of NB-SWNT. B-SWNT and NB-SWNT were diluted to a final concentration of 10 mg/L. NO solution was generated by bubbling 100% NO gas through deoxygenated PBS using a method similar to one previously described [9]. NO concentration was calculated through the use of a UV-Vis second order derivative spectroscopy technique using HRP as the active component which has been previously reported [273]. NO was added to SWNT samples at a final concentration of 60 uM and quenching was recorded with an exposure time of 200 ms. Aggregate curves were constructed (n=3) and displayed (Figure 2-2d). Inspection of quenching rates indicates that biotinylation had little effect on quenching capacity with B-SWNT and NB-SWNT samples reaching an average of 90% quenching, following the addition of NO, after 25 and 24 seconds respectively.

2.3.2 Generating Avidin and APTES Derivatized Surfaces

Contact angle measurements were taken stepwise during surface development (Figure 2-3a,b,c). Piranha treated slides, 3-GPTMS functionalized, and avidin functionalized slides provided contact angle measurements of <5°, 58.4°, and 29.6° respectively (n=5, ± 4°). Piranha treatment, which is responsible for the formation of hydroxyl groups showed an extremely low contact angle which is consistent with literature values [277, 278]. 3-GPTMS functionalization induced a characteristic increase in contact angle [279]. Finally, the addition of avidin lowered the contact angle due to its hydrophilicity compared to 3-GPTMS [271]. All contact angles indicated proper functionalization during each step of the fabrication process.

In order to further confirm functionalization, XPS was employed to observe key atomic spectra, specifically the C1s, N1s, O1s and Si2p chemical peaks (Figure 2-3). Upon piranha treatment, a small C1s peak is observed which is indicative of background adventitious carbon levels, no nitrogen peak is observed, and strong Si2p and O1s peaks are observed from the underlying SiO_2 substrate. Following 3-GPTMS functionalization an increase in carbon content is observed at ~284.1 eV which may be attributed to the C-C bonds in the arm of the silane and at a shoulder peak of ~285.8 eV which corresponds with the C-O bonds of the silanes epoxide ring, no nitrogen peak is observed, and the Si2p/O1s peaks show a reduction from piranha treatment which can be attributed to presence of the silane (XPS is a highly depth dependent technique). Finally, when avidin is derivatized on the surface the existing C-C and C-O peaks increase greatly since, like most proteins, avidin is carbon dense, while an additional peak at ~ 287.7 appears which

is attributed to the C=O bonds of avidins peptides. A nitrogen peak also appears at ~ 399.5 eV which can be contributed to the C-NH_2 groups found in the amino acids of avidin, and the Si2p/O1s peaks are even more diminished due to the protein's presence on the surface. Atomic percentage values were also calculated using Avantage software and are in good accordance with atomic spectra (Table 2-2).

APTES surfaces were generated similarly to the way that 3-GPTMS surfaces were built. Contact angle measurements obtained APTES functionalized surfaces (n=5, ± 4°) provided a contact angle of 51.8° demonstrating its successful deposition on the glass surface (Figure 4a) [280]. The C1s spectra from APTES indicates an increase in carbon following APTES deposition via a peak at ~284.4 eV, attributable to the C-C bonds found in the silane arm. Following APTES functionalization a nitrogen peak is generated at ~ 399.3 eV which may be attributed to the aminopropyl head of APTES. The O1s and Si2p peak both show decreases in intensity indicative of APTES derivatization. Atomic percentages were also calculated and are in good accordance with XPS spectra (Table 2-3).

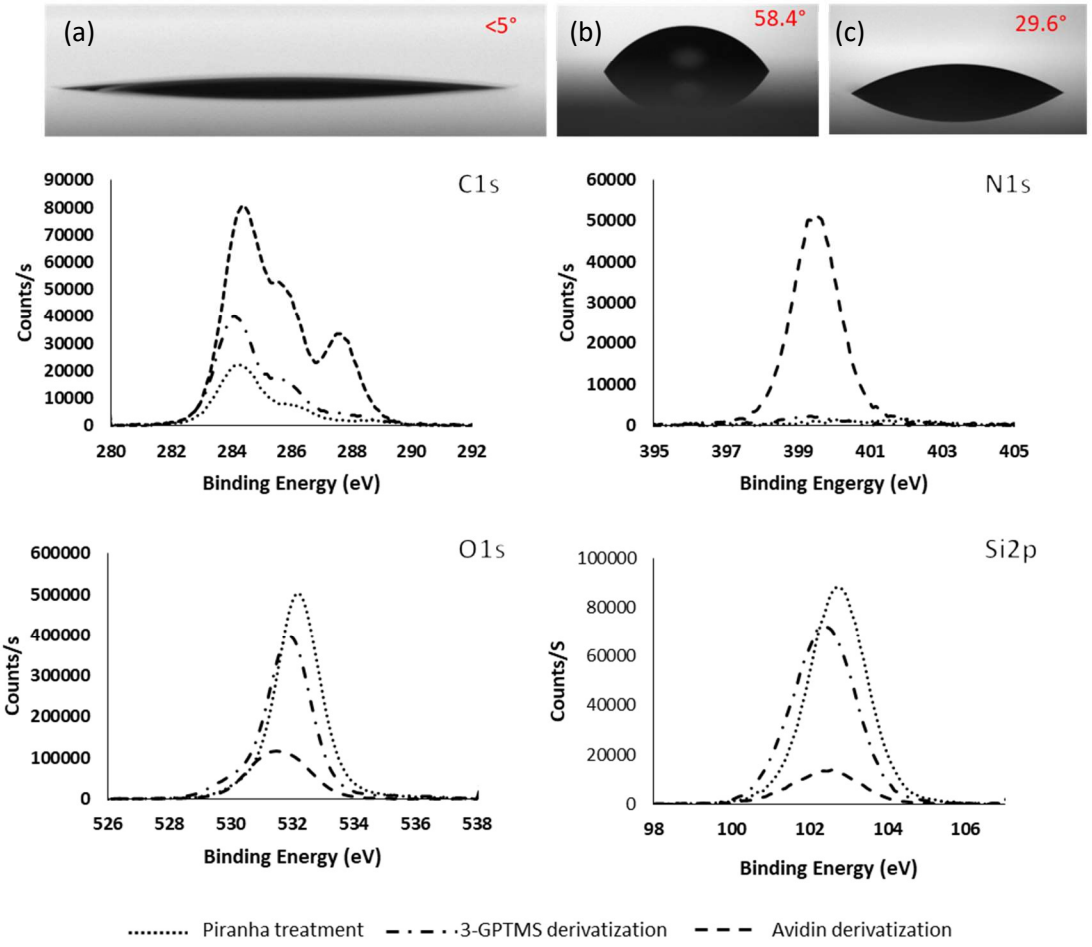

Figure 2-3: Generating avidin derivatized substrates (a) Piranha treated slides, demonstrated a contact angle of <5° which is consistent with glass substrates treated in this manner. (b) GPTMS treated slides, center, show a characteristic increase in contact angle of 58.4°. (c) Avidin treated slides showed a reduction in contact angle to 29.6° which can be attributed to avidin's hydrophilicity. (XPS peaks) The C1s clearly demonstrates an increase in the total carbon after GPTMS and avidin functionalization indicating their presence on the surface. The N1s peak showed no substantial peaks until avidin functionalization indicating avidins presence on the surface. Both the O1s and Si2p peaks demonstrate shielding effects as the addition of silane and later avidin reduce the signal intensity from the underlying SiO_2 framework.

Table 2-2: Atomic percentages for avidin derivatization. Atomic percentages of the C1s, N1s, Si2p, and O1s chemical states for each step in the avidin derivatization process. Percentages are in good accordance with spectral observations showing increases in carbon and nitrogen upon avidin treatment and decreases in silicon and oxygen indicating shielding

Derivatization Step	**Atomic Percent**			
	C1s	**N1s**	**Si2p**	**O1s**
Piranha	8.95	0.68	26.91	63.46
Epoxy Silane	16.75	0.67	57.07	25.5
Avidin	54.14	12.93	26.27	6.66

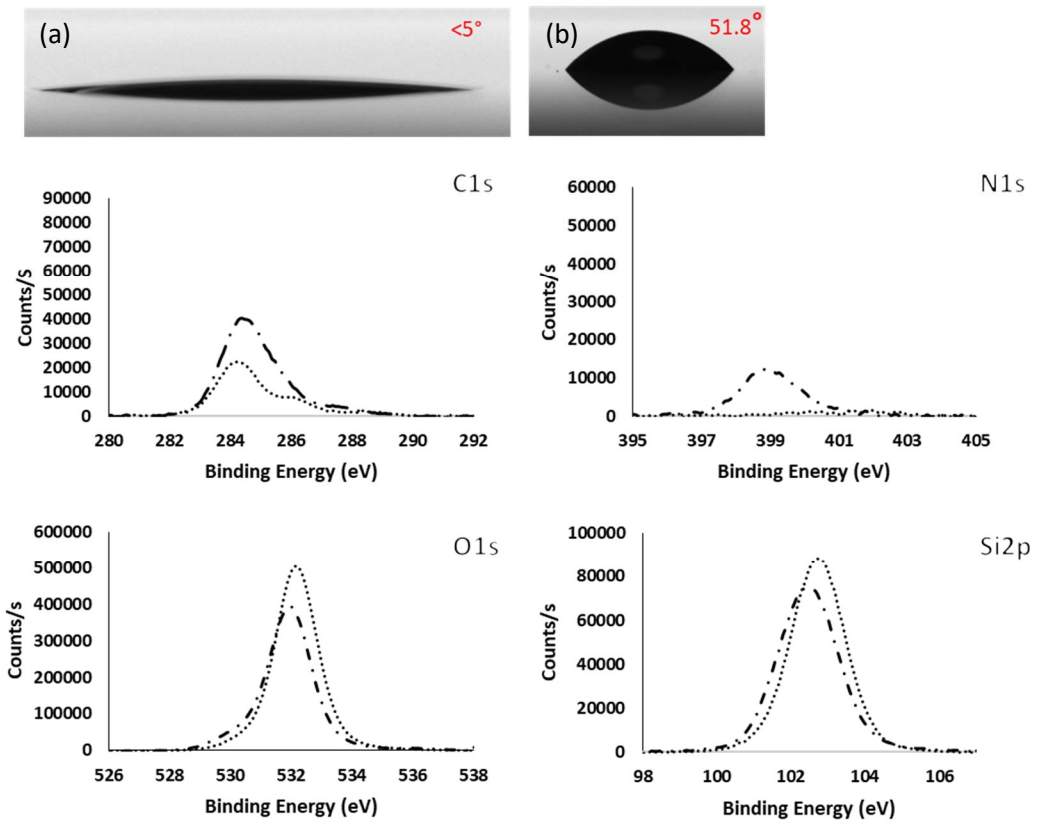

Figure 2-4: Generating APTES derivatized substrates (a) Piranha treated slides, demonstrated a contact angle of <5° which is consistent with glass substrates treated in this manner. (b) APTES treated slides, show a characteristic increase in contact angle of 51.8°. (XPS peaks) The C1s peak clearly demonstrates an increase in the total carbon content after APTES functionalization, which can be attributed to the arm of the silane. The N1s peak showed no substantial peaks until APTES functionalization which can be attributed to the aminopropyl head of ATPES. Both the O1s and Si2p peaks demonstrate shielding effects as the addition of the silane reduces the signal intensity from the underlying SiO_2 framework.

Table 2-3: Atomic percentages for APTES derivatization. Atomic percentages of the C1s, N1s, Si2p, and O1s chemical states for each step in the APTES derivatization process. Percentages are in good accordance with spectral observations showing increases in carbon and nitrogen upon APTES treatment and decreases in silicon and oxygen indicating shielding.

Derivatization Step	**Atomic Percent**			
	C1s	**N1s**	**Si2p**	**O1s**
Piranha	8.95	0.68	26.91	63.46
APTES	15.77	2.98	25.74	55.51

2.3.3 Demonstrating Surface Functionality

We next sought to test the functionality of the platform. In order to accomplish this goal 30 mg/L B-SWNT and NB-SWNT were applied to intermediate substrates (Untreated, Piranha Treated, and 3-GPTMS Derivatized) used during the derivatization process and completed substrates (APTES/Avidin) for a period of 24 hours. Fluorescent readings were collected at 5 locations across the surface of the treated area (Figure 2-5) and three slides were sampled per condition in order to determine an average fluorescence per condition (n = 3, s = 5). Significance was determined using a one-way ANOVA with Tukey's multiple comparison test (prism software).

The Intermediate substrates showed little fluorescence, often attaining values just above background indicating that they do not contribute significantly to the long-term retention of SWNT on the surface.

Avidin and APTES derivatized surfaces showed a significant increase in fluorescence compared to intermediates for both B-SWNT and NB-SWNT ($p \leq 0.0005$). No significant difference in fluorescence intensity could be determined between B-SWNT + APTES, NB-SWNT + APTES, and Avidin + NB-SWNT. These results indicate that (1) biotinylation does not affect the electrostatic properties of SWNT and (2) the use of avidin for the electrostatic/non-specific deposition of NB-SWNT produces results similar to that of APTES when considering fluorescence intensity.

In addition to outperforming intermediate layers, Avidin + B-SWNT showed a significant increase in fluorescence intensity compared to all of the electrostatic/non-

specific tests ($p \leq 0.0001$) more than doubling the next highest fluorescence intensity indicating that the avidin-biotin interaction produces enhanced SWNT deposition.

Despite Avidin + B-SWNT having a much higher concentration of SWNT attachment, we continued to study those combinations which produced significantly more fluorescence than background (APTES + NB-SWNT, APTES + B-SWNT, Avidin + NB-SWNT, and Avidin + B-SWNT).

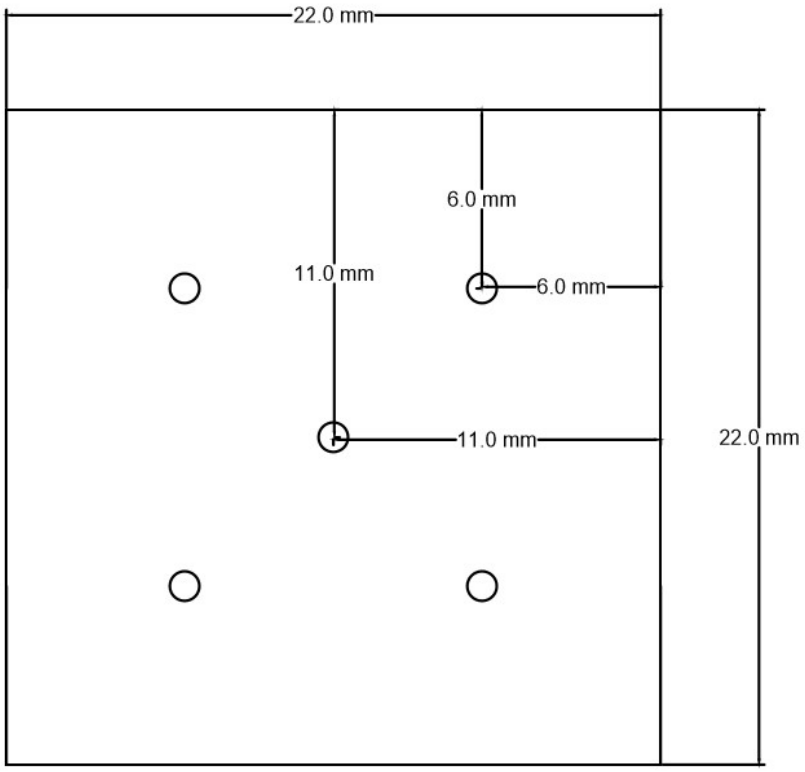

Figure 2-5: Fluorescent imaging locations. A 22 X 22 mm section of glass slide was treated with Avidin and SWNT by placing the solution under a coverslip and incubating for 24 hours. The figure above demonstrates the locations imaged in the treated area where circles are the locations imaged. 5 subsamples per slide were always taken. Samples were moved in slightly from the edges to prevent edge effects from skewing results

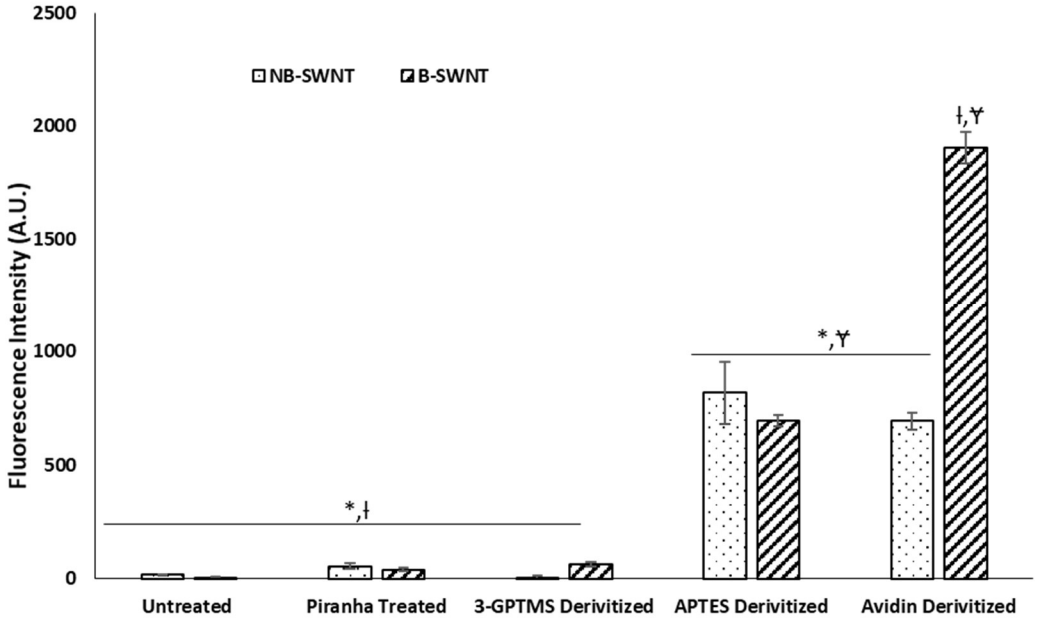

Figure 2-6: Demonstrating surface specificity. 30 mg/L NB-SWNT and B-SWNT was applied to substrates required as intermediates in the derivatization processes and completely derivatized surfaces. Intermediate surfaces showed little to no retention of SWNT while APTES and avidin showed a significant increase in SWNT retention. The SWNT/substrate combinations of APTES + NB-SWNT, APTES + B-SWNT, and Avidin + NB-SWNT showed no significant differences, while the Avidin + B-SWNT condition showed over a significant increase in fluorescence compared to all electrostatic and non-specific conditions indicating that the addition of biotin does enhance SWNT retention.

2.3.4 SWNT Loading Performance

We next chose to explore the relationship between SWNT concentration and loading performance using our isolated SWNT/substrate conditions. SWNT concentrations of 10, 20, 30, 40, and 50 mg/L were applied to their respective surfaces. Fluorescent intensity values were collected as previously stated and average fluorescence values calculated (n=5, s=5). Samples were grouped based on the SWNT concentration they occupied, and an ordinary one-way ANOVA analysis conducted using Prism.

Multiple comparison tests were conducted using the Tukey method and indicated that at 30, 40, and 50 mg/L SWNT the Avidin + B-SWNT combination produced significantly more florescence than any of the other 3 combinations ($p<0.02$, $p<0.01$, $p<0.005$) (Figure 2-3a). Moreover, the remaining three conditions showed a stagnation of intensity across concentration indicating that they may already be saturated at concentrations as low as 10 mg/L. This indicates that the avidin-biotin bond can be used to increase the quantity of SWNT at the surface, which would allow researchers to decrease laser intensity levels while achieving the same levels of fluorescence provided by the current standards.

We next sough to explore the effects of the avidin-biotin bond on SWNT distribution to ensure that the gains in SWNT quantity at the surface did not harm the high quality distribution already enjoyed by electrostatic deposition methods [8, 73]. In order to accomplish this goal images were analyzed via two methods. In the first method images were normalized with respect to their maximum intensity forming a matrix (CO) in which values ranged from 0 (no fluorescence) to 1 (maximum fluorescence). Next a single-level 2-D wavelet decomposition was applied to the images using the Harr wavelet. This provided a matrix of detail coefficients in the horizontal (CH), vertical (CV), and diagonal (CD) directions for each SWNT image. We then used the percent energy of the pixels being partitioned into the diagonal wavelet component as the index to assess randomness. Samples were groups based in the concentration they occupied, and a one-way ANOVA analysis performed as previously described. Using this method, no significant differences in overall smoothness could be determined for all SWNT/substrate combinations (Figure 2-7b). These results indicate that the increased SWNT quantity at the surface as a result of the avidin biotin bonding mechanism did not

harm the distribution of SWNT compared to electrostatic and non-specific mechanisms. In the second method we used the arithmetical mean deviation (Ra) model. Images were again normalized to their maximum intensity values. Ra was calculated by subtracting each pixel's intensity (y_i) in an image from the average intensity of the whole image ($\bar{y}$) and finding the absolute value. The resulting deviations from the average intensity were summed and divided by the total number of pixels. One-way ANOVA analysis was then applied as previously described. Results again showed no significant differences in distribution quality for any SWNT/substrate combinations (Figure 2-7c). Sample images show similar distributions across all combinations (Figure 2-7d,e,f,g). These results further confirm that the increased SWNT quantity at the surface did not harm the quality of the distribution already experienced by electrostatic and non-specific binding mechanisms.

$$\boldsymbol{Indexing\ value} = \frac{\sum_{i=1}^{n}(\boldsymbol{CD_i})^2}{\sum_{i=1}^{n}(\boldsymbol{CO_i})^2}$$

$$\boldsymbol{Ra} = \frac{\mathbf{1}}{\boldsymbol{number\ of\ pixels}} \sum_{i=1}^{n} |\bar{\boldsymbol{y}} - \boldsymbol{y_i}|$$

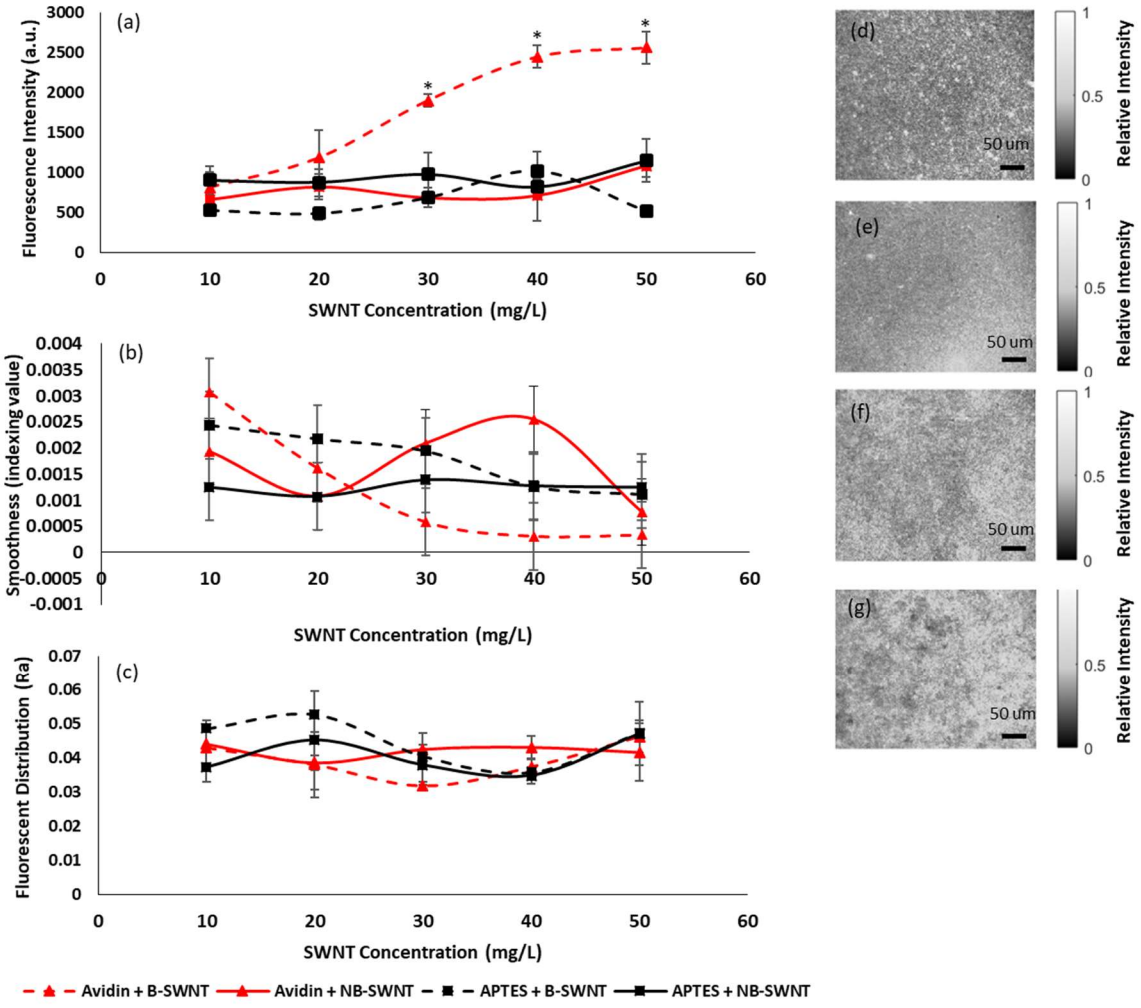

Figure 2-7: SWNT loading and distribution properties (a) SWNT loading was determined from 10 – 50 mg/L for all SWNT/substrate combinations. Concentrations of 30 mg/L and greater produced significant increases in loading capacity for the Avidin + B-SWNT combination when compared with all other combinations. (b) One measure of SWNT distribution was determined via the percent of total energy in the diagonal wavelet (Indexing value). (c) A second measure of SWNT distribution was determined via the arithmetic average roughness (Ra). Indexing and Ra values showed no significant changes between all substrate/SWNT combinations indicating a smooth loading of SWNT across all SWNT concentrations. (d,e,f,g) Representative images of Avidin + B-SWNT, Avidin + NB-SWNT, APTES + B-SWNT, APTES + NB-SWNT respectively.

2.3.5 Immobilized SWNT Spectral Properties, Longevity and Sensor Response

When SWNT deposition is used, it is frequently in an attempt to determine the relative concentration of cellular signaling molecules or proteins. As a result, the SWNT adhered to the surface is often under stresses typical to cell culture such as changing media. The method of SWNT adherence must therefore be robust enough to withstand these conditions over long periods of time. We examined the ability of any SWNT functionalized surface to withstand long culturing periods.

In order to simulate the physical stresses of cell culture, slides were prepared using 10 mg/L SWNT and placed in individual slide holders with 4 mL of nanopure water so that the surface was completely covered. Every day the supernatant was completely removed and replaced with fresh nanopure water. We tracked the loss of SWNT from the surface of the various platforms over the course of 10 days. Fluorescent readings were collected as previously described and the percent of initial fluorescence was calculated (n=5, s=5). Samples were grouped based on the day they were collected, and an ordinary one-way ANOVA conducted in conjunction with Tukey's multiple comparison test. No sample could be found which consistently maintained more SWNT on the surface over the course of 10 days although those conditions which used avidin substrates did maintain the highest average SWNT fluorescence at the end of the study (Figure 2-8a). These results indicate that the avidin-biotin bind does not negatively impact the platform's ability to resist physical disturbances typical in cell culture when compared to the currently available electrostatic and non-specific deposition mechanisms.

An important aspect in the development of the platform is SWNT's sensing capabilities following immobilization. Existing surface decoration methods of SWNT deposition show short response times compared to matrix immobilization methods. It is important that the avidin biotin interaction not interfere with the response time of the sensor and that it continues to perform similarly to existing surface decoration methods that are based on electrostatic and non-specific deposition, therefore the response of each platform to NO was tested. Fluorescence intensity was monitored (500 ms exposure time) for each sample before and after the addition of 60 uM NO (n =5). Quenching curves were collected, aggregated, normalized, and smoothed using a Savitzky-Golay smoothing function (order = 3, frame length = 21). Avidin + B-SWNT, Avidin + NB-SWNT, APTES + B-SWNT, and APTES + NB-SWNT all showed remarkably similar quenching patterns with each platform reaching 90% quenching, following the addition of NO, after 18, 17, 18, and 18 seconds respectively (Figure 2-8b). This indicates that the avidin biotin bond is not hindering sensor responsiveness and the platform continues to respond similar to the current surface decoration methods.

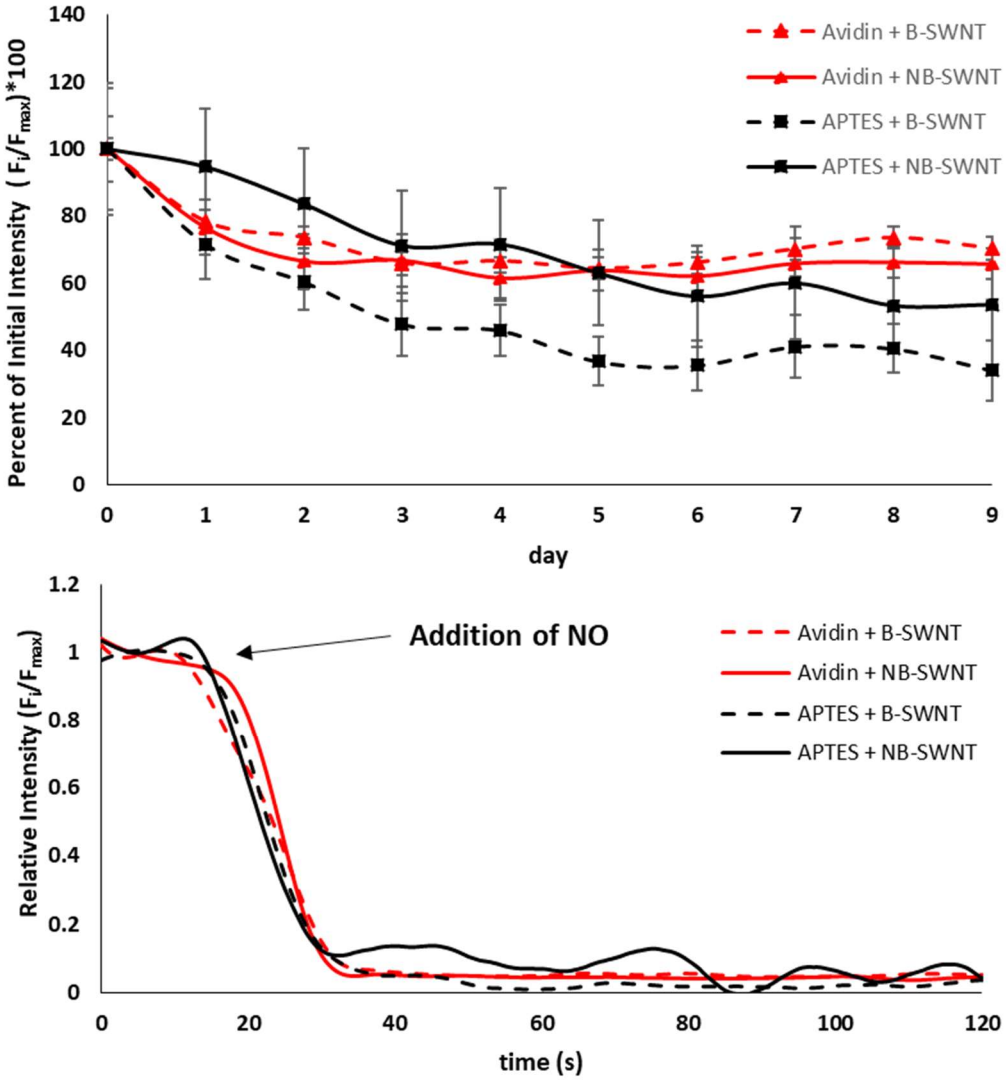

Figure 2-8: SWNT longevity and analyte responsiveness. (a) 10 mg/L B-SWNT and NB-SWNT was applied to APTES and avidin substrates. Slides were stored in individual slide holders with 4 mL of nanopure water which was replaced every day. Fluorescence intensity values were tracked over the course of 10 days. No sample could be found which consistently outperformed all others in terms of SWNT retention, indicating that all samples degraded similarly. (b) 10 mg/L B-SWNT and NB-SWNT was applied to APTES and avidin surfaces and quenched by 60uM NO (final concentration). All samples showed similar quenching results indicating that the method of deposition had little impact on sensor performance.

2.4 Conclusions

This work highlights the first use of a covalently tethered avidin molecule for the deposition of non-biotinylated and biotinylated DNA-SWNT on a glass surface. We demonstrated that biotinylation of SWNT using biotinylated DNA was not only possible, but also did not affect the behavior of the SWNT sensors. A scheme for the derivatization of surfaces with a covalently linked avidin molecule was determined and proved using a combination of contact angle and XPS analysis. Compared with a traditional method of SWNT deposition (APTES) the use of an avidin-biotin bond produced significant increases in SWNT retention at 30, 40, and 50 mg/L SWNT without damaging the spatial distribution, longevity, or quenching capacity. Improved loading capacity could have immediate benefits for the study of *ex vivo* and *in vitro* samples including decreased laser intensity resulting in fewer effects on the sample and the ability to decrease the exposure time resulting in increased sample sizes. This method may also be able to enhance the binding efficacy of similar DNA-SWNT sensors allowing for the production of multi-sensor arrays which are spatially localized. Future applications should test these hypotheses using live cell samples.

CHAPTER 3

Conclusions and Future Directions

3.1 Thesis Conclusions

In this thesis, the quantity of SWNT deposited on a glass slide was dramatically increased using a highly characterized avidin-biotin bonding mechanism without damaging the positive aspects of previous deposition mechanisms, including distribution and response time. The enhancement requires the biotinylation of DNA oligos prior to their wrapping of raw SWNT to form biotin-DNA-SWNT complexes, and the covalent linkage of avidin to a glass surface through an epoxy-silane intermediate. This thesis focused on improving the quantity of SWNT deposited on a glass surface using the NO sensing DNA-SWNT complex as a proof of concept due to its simplicity and immediate application, and because many other SWNT sensors also employ DNA wrappings meaning this method could easily be extended to enhance their deposition as well. These findings demonstrate the potential for avidin-biotin based deposition techniques to supersede traditional methods of deposition, which employ electrostatic or non-specific interactions, and provides researches with an easy to follow protocol for the deposition of their own DNA-SWNT sensor complexes.

The enhancement of DNA-SWNT deposition efficiency and total mass loading will have an immediate impact on the research community, making avidin-biotin deposition superior to electrostatic and non-specific deposition methods. More specifically, an increase in deposition efficiency will reduce costs for labs since less SWNT will be required to achieve similar results to previous methods. The increase in

total SWNT loading will also decrease laser intensity requirements to excite SWNT sensors for imaging purposes *in vitro*, which could decrease the potentially negative effects associated with sample heating and cellular photo-stimulation [281]. As an alternative to decreasing the laser intensity, researchers could also reduce the exposure time needed to capture data, thus decreasing the duration of cell exposure to laser light and time spent out of the incubator. Decreasing exposure time can also increase sample collection rates allowing for higher temporal resolution. Moreover, the increased fluorescence from the surface compared to current electrostatic and non-specific deposition strategies could allow for lower microscope magnifications to be used, increasing the viewing area and permitting the visualization of large scale intercellular signaling events.

In addition to its *in vitro* applications this method of SWNT deposition may have *ex vivo* applications as well. There is currently much interest in the detection of biologically relevant molecules from biological fluids (urine, blood, plasma, and saliva) as it is minimally invasive, low cost, generally accepted by patients, and easily repeated [282]. Molecules such as lipids, proteins, genetic materials, and ROS/RNS species can provide clinicians with information vital to the detection and progression of many disease states including: cardiovascular disease, pregnancy complications, viral and bacterial infections, cancer, and inflammatory disease [283-288]. Current methods for the detection of molecules of interest rely on a range of techniques including immunological analytical methods, quantitative PCR, chromatographic techniques, and colorimetric indicators [289-292]. Many of these procedures are time intensive or require extensive purification procedures, even more importantly, they require multiple reagents and

expensive equipment. DNA-SWNT complexes are capable of detecting all of the molecules listed above and require a single imaging modality. Unfortunately, many SWNT sensors cannot be mixed with one another and still provide valuable information to the researcher since the SWNT occupy similar excitation and emission wavelengths. However, the method of SWNT deposition outlined in this thesis could be used to synthesize microarrays which would keep SWNT sensors separate. SWNT microarrays could provide rapid, direct detection of analytes of interest from a single sample, thus saving the healthcare provider money and decreasing the volume of sample taken from the patient.

While the findings of this thesis provide researchers with a method to dramatically increase SWNT deposition efficiency on glass substrates, the protocol should be further optimized. Moreover, there are additional questions which still require investigation, including the effects of expanding this method to additional DNA-SWNT sensor complexes, the effects of a SWNT sensor substrate on cellular health, behavior, and performance, and the optimal SWNT surface concentration for performing extracellular signaling studies. Recommended studies for the continuation of SWNT deposition enhancement are described in detail below.

3.2 Future Studies: Additional Optimization of Avidin-Biotin Based SWNT Deposition

While the protocol developed in this thesis was successful in imparting active biotin to functional SWNT sensors for the purpose of immobilization, covalently immobilized avidin, and successfully improved SWNT loading over previous methods several facets of the process require additional study and optimization. Areas of this process which still require study include determination of the optimal degree of biotinylation, the use of avidin isoforms, increasing surface area to further enhance SWNT loading, and derivatization reaction times.

3.2.1 Degree of Biotinylation

The degree of biotinylation (i.e. the number of biotin per SWNT) could drastically alter the amount of SWNT present on the platform surface and the stability of the final product. The biotinylation scheme used in this thesis resulted in approximately 6 biotins per SWNT, while avidin proteins have 4 available binding sites. If all biotin moieties bind to an avidin, there is an average of 0.67 SWNT/avidin. In theory, increasing the degree of biotinylation could allow a single SWNT to bind additional avidin molecules and increase its stability on the surface as its anchoring mechanism becomes further distributed. Assuming an increase in stability is desired and all 31.25 DNA locations are biotinylated, this would result in an average of 0.128 SWNT/avidin and an 80% loss of

SWNT present on the surface. Thus, by enhancing its stability, increased biotinylation would also limit the improved deposition efficiency detailed in this thesis. The converse is also true, decreasing biotinylation could allow for increased deposition by allowing, at a maximum, 4 SWNT per avidin molecule and an increase in efficiency gains. However, the increased reliance on a single anchoring site would likely lead to decreased long-term SWNT stability. The ideal properties of any surface are often dependent upon the researchers needs and, in some instances, researchers might be willing to sacrifice stability for increased deposition efficiency or vice versa. The behavior of the sensor should be catalogued at various degrees of biotinylation and a model developed which would allow researchers to select their desired properties ahead of time.

3.2.2 Exploring Avidin Isoforms

The use of avidin isoforms (streptavidin and neutravidin) should be explored. Avidin, which is produced from egg whites, was used in this thesis because it has been highly characterized, is readily available, and is relatively inexpensive. However, avidin is known to encourage some non-specific adsorption due to its high isoelectric point (pI ~10) and oligosaccharide component [293, 294]. In fact, we attribute the presence of some SWNT retention in this thesis to the electrostatic interactions between the cationic avidin and the negatively charged backbone of DNA. Although it may be beneficial under certain circumstances to enhance SWNT binding with the addition of an electrostatic component, the cationic nature of avidin could lead to unintended

interactions between avidin and negatively charged molecules common to cell culture, such as cell membranes [293, 295]. Streptavidin is a non-glycosylated form of avidin produced by the bacterium *Streptomyces avidinii* which has a similar binding site for biotin and a pI of ~5-6 [293, 294]. Neutravidin is a protein that has been chemically deglycosylated and has a pI of 6.3 [295]. The removal of the sugar groups and lowering of the pI could result in less non-specific adsorption, which may provide better results for cell culture work. As a result, preliminary data was collected to determine if NeutrAvidin could be covalently bound to glass substrates using the same epoxysilane intermediate method which was utilized for the deposition of avidin in chapter 2. XPS spectra were collected across the C1s, N1s, O1s, and Si2p peaks for each step in the procedure (Figure 3-1). Following piranha treatment, a small free carbon peak can be observed, which is considered background carbon, no nitrogen peak is observed, and O1s and Si2p peaks are strong due to the SiO_2 glass substrate. Following 3-GPTMS derivatization, an increase in carbon content is observed, which is attributable to the carbon in the arm of the silane, no N1s peak is observed, and both the O1s and Si2p peaks show a decrease in intensity since the silane shields the SiO_2 surface. Finally, following NeutrAvidin functionalization a large C1s peak is observed, which may be attributed to the carbon found in NeutrAvidin, a N1s peak is observed which can be attributed to primary amines in the protein, and the O1s and Si2p peaks are further decreased as a result of increased shielding from NeutrAvidin. These results indicate that NeutrAvidin can be covalently coupled to the surface of a glass slide in a manner similar to avidin, but further work is required to ensure SWNT binding occurs and compare its efficacy, and distribution to previously described methods.

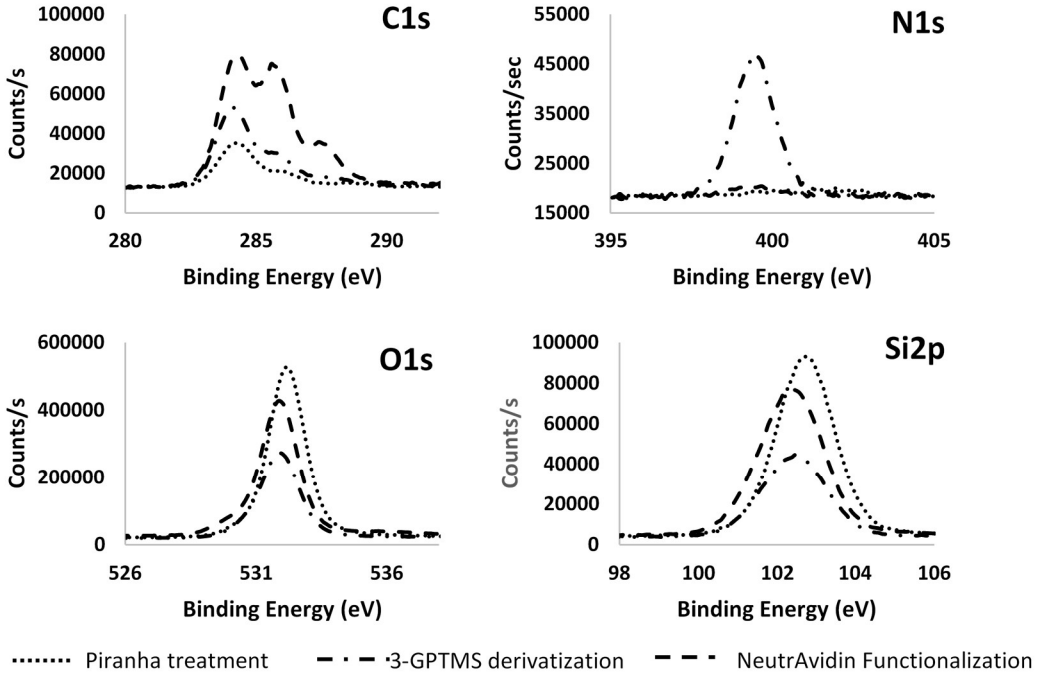

Figure 3-1: Generating NeutrAvidin derivatized surfaces. XPS Spectra for the C1s, N1s, O1s, and Si2p atomic states demonstrate proper NeutrAvidin Functionalization following the methods developed in chapter 2.

3.2.3 Increasing Available Surface Area

Despite optimizing the degree of biotinylation and the avidin isoform used, this platform may still not produce enough SWNT deposition for some unforeseen applications. One method to increase deposition further would be to increase the surface area of the underlying glass (SiO_2) framework through the use of nanoporous SiO_2 films. Nanoporous SiO_2 films can readily be created on the surface of existing glass substrates through the use of an inverse opal technique [296-298]. Briefly, colloidal polymer latex

nanospheres, such as polystyrene (PS) or poly (methyl methacrylate) (PMMA), are allowed to self-assemble on the surface of a glass slide through an evaporative process, creating a crystal film [296-298]. A sol-gel solution is applied, infiltrating the crystal film and acting as a precursor for the creation of the SiO_2 nanopores [299-303]. The nanospheres are then removed, typically by calcination, and an inverse opal film is generated [271, 304] (Figure 3-2). The inverse nonporous film can drastically increase area available for functionalization, allowing additional SWNT to be adhered to the surface using the techniques developed in chapter 2.

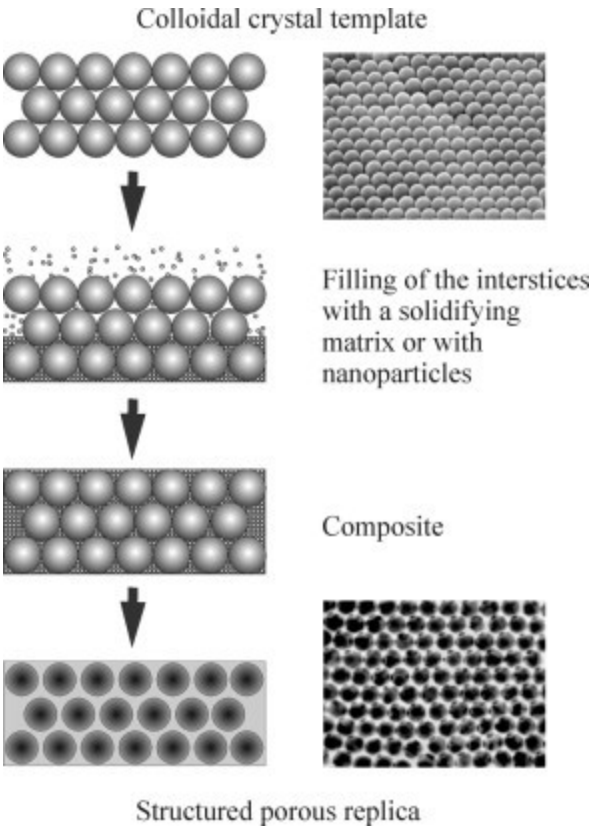

Figure 3-2: Creating inverse opal films. The general procedure for creating a porous surface through the inverse opal technique are (1) generating a colloidal crystal (2) filling the open spaces of the matrix with nanoparticles (3) removing the colloidal crystal. Reprinted from [301] with permission from Elsevier.

3.2.4 Improving Reaction Times

The timeline for each processing step in the development of the SWNT platformed in this thesis should be evaluated. The method utilized in this paper was a modified version of the one found in the popular handbook *Protein Microarrays* and a recent paper by Zhanjun Yang et al. [15, 271]. For this thesis, timelines for certain derivatization steps were conservative, resulting in a derivatization process which required 5 days to complete. Many laboratories may consider a 5-day preparation time to be too long. If the time period for platform development is decreased without altering performance, then increased research flow/progress could be achieved. While the issue of extensive preparation time can be partially combated with increases in the batch size, this may be impractical for smaller labs, therefore a new study should be performed to accurately characterize the necessary reaction times to achieve optimally derivatized slides. The derivatization of glass substrates with 3-GPTMS has been extensively studied [305-307] and new timelines for its derivatization might be determined from the literature. However, the addition of avidin to the 3-GPTMS monolayer remains understudied at best, and the necessary reaction times for biotinylated SWNT to achieve maximal saturation on the avidin surface has not been studied at all. Proper reaction times could be determined using a variety of surface characterization techniques including ellipsometry, XPS spectroscopy, and AFM. By focusing on the timelines required for avidin derivatization and subsequent SWNT functionalization entire days could be removed from the protocol, allowing researchers to accelerate their project timelines.

3.3 Future Studies: Deposition of Additional Sensors

This thesis focused on the 6,5 d$(AT)_{15}$ SWNT sensor as a proof of concept for the deposition of DNA-SWNT complexes using the avidin-biotin binding mechanism. Additional sensors of different chirality's and DNA wrappings must be tested and optimized before they can be used. Moreover, following the optimization of many sensors, the platform should be used in a practical manner to demonstrate its versatility, such as the development of a microarray.

3.3.1 Optimizing Additional DNA-SWNT Complexes

Although the DNA wrapped SWNT share similar physical properties, they are not identical. Many chirality's of SWNT are used for sensors and many DNA wrappings are commonly used. For example, the sensor responsible for the detection of H_2O_2 is a 7,6 d$(GT)_{15}$ SWNT, while the sensor responsible for lipid detection is a 9,4 d$(CTTC_3TTC)$ SWNT [80, 308]. It is not clear how DNA oligos of variable bases or length might affect the sensor platform. Recently, Robert Nißler et al. demonstrated a practical method for the determination of the number of oligos per SWNT of various nucleotide sequence and length [276]. In doing so, it was demonstrated that the number of DNA oligos per 6,5 SWNT was highly dependent upon the length of the oligo and its sequence. Because the number of biotin moieties present on SWNT is linked to the number of DNA wrappings, this would suggest that the degree of biotinylation between sensors would also be highly

variable without carefully tailoring the wrapping procedure to each sensor. Unfortunately, Nißler's study focused only on 6,5 SWNT and a handful of DNA oligos, so many of the more useful DNA-SWNT complexes have yet to be characterized. However, the method developed by Nißler could easily be extended to determine the number DNA oligos wrappings for the varieties of DNA-SWNT complexes used for sensors. Once the number of oligos per SWNT is known, the ratio of biotinylated to non-biotinylated DNA oligos can be tailored so that each sensor will have a similar number of biotin per SWNT.

3.3.2 Developing a Sensor Microarray

Following optimization of desirable sensors, the field would benefit from a practical application of the avidin-biotin immobilization scheme. One such application would be the immobilization of multiple DNA-SWNT sensors to form a microarray. Microarrays are essential for the high throughput analysis of biomolecule expression. The use of the avidin-biotin bonding mechanism could easily be used to generate a label free microarray using various DNA-SWNT complexes. Spotting, microprinting, or masking of the avidin derivatized surface with the sensors of the researcher's choice all have the potential to create viable microarrays. The use of SWNT sensors for the development of a microarray has already been pursued by Dong et al. [74]. However, Dong's method of deposition required matrix immobilization of the sensors, which could alter sensor response time as previously discussed. Surface decoration though the process developed

in this thesis could significantly decrease microarray response times and increase the variety of sensors that could be utilized.

3.4 Future Studies: Cellular Applications

3.4.1 Effects of SWNT Substrates on Cellular Behavior

Although the effects of DNA-SWNT complexes on animals have been shown to be minimal [5, 80, 151, 162, 163], the effects on cells remains less certain [1], primarily due to the unknown status of DNA-SWNT's interactions with common indicators of cell health. Raw SWNT has been shown to interact with a host of assays including Commassie Blue, Alamar Blue™, Neutral Red, MTT and WST-1, primarily though hydrophobic interactions [167, 168]. However, the DNA-wrapping on SWNT sensors makes them hydrophilic and may decrease or prevent hydrophobic interactions from occurring. A study should be conducted to determine the effects of DNA-wrapped SWNT on common cell health assays when SWNT is in solution and when SWNT is adhered to the surface of a substrate using the avidin-biotin bonding mechanism. A series of studies should then be conducted to determine the effects of SWNT derivatized surfaces on cellular adhesion, proliferation, viability, and cytoskeletal development across a variety of cell types using those assays with which DNA-SWNT does not interfere.

Although cellular indicators are necessary for a more in depth understanding of the effects of SWNT surfaces on cellular behavior, preliminary work to determine this platform's ability to serve as a viable cell culture substrate can begin immediately.

Recently, Xiaoke Zhang et al. demonstrated that SWNT polysaccharide wrappings, which produced a high zeta potential (surface charge) and a low contact angle, produced the greatest benefits to cellular growth in comparison to raw and oxidized SWNT [309]. As a result of these findings, contact angle measurements were taken using the platform developed in chapter 2 (Figure 3-3). An average contact angle of 47.7° was achieved, which is substantially less than the 81° achieved by Xiaoke Zhang et al. Moreover, avidin's highly cationic nature may prove beneficial in enhancing the zeta potential of this platform. These results indicating that adhered DNA-SWNT complexes have potential for use as cellular growth substrates.

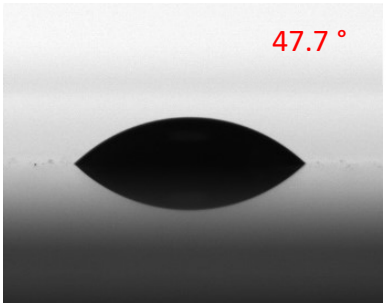

Figure 3-3: Contact angle achieved by SWNT derivatized surfaces. 6,5 biotinylated $d(AT)_{15}$ adhered to an avidin derivatized substrate displaying an aggregate contact angle of 47.7 ° well below the 81° achieved by Xiaoke Zhang et al. and indicating the potential for good biocompatibility.

3.4.2 High Resolution Imaging of Cellular Signaling

This thesis did not include high resolution imaging of cellular signaling molecules and proteins which were produced directly by cells, but it is a logical next step once the effects of the platform on cell health have been determined. The 6,5 $d(AT)_{15}$ SWNT sensor would be an interesting candidate for initial testing since it was previously used to

quantify intracellular NO concentrations [69]. The cell lines and stimulants used for the study of intracellular NO could be used to study extracellular NO concentrations. In fact, much of the work which has already been developed for the use of a variety of SWNT as intracellular sensors could be co-opted for use in extracellular studies.

3.5 Final Thoughts

The outcomes of this thesis, demonstrated in Chapter 2, illustrate the potential of the avidin-biotin bond to enhance binding specificity and concentration of fluorescent single walled carbon nanotubes on a glass substrate. Chapter 3 has suggested many future studies which will further enhance SWNT binding, reduce platform preparation time, provide additional substrate options to researchers, determine the effects of SWNT surfaces on cellular health, and demonstrate the platform's practical value.

Increasing SWNT deposition could provide researchers with a new tool to more accurately study cellular signaling and communication. Because cellular signaling underpins almost every coordinated biological process its understanding is critical to the understanding and treatment of disease. Providing researchers with this tool may ultimately result in new treatments and monitoring devices for clinicians and patients.

REFERENCES

1. Jena, P.V., et al., *A carbon nanotube optical reporter maps endolysosomal lipid flux.* ACS nano, 2017. **11**(11): p. 10689-10703.
2. Jeng, E.S., et al., *Detection of a Single Nucleotide Polymorphism Using Single-Walled Carbon-Nanotube Near-Infrared Fluorescence.* Small, 2010. **6**(1): p. 40-43.
3. Harvey, J.D., et al., *HIV Detection via a Carbon Nanotube RNA Sensor.* ACS sensors, 2019.
4. Jeng, E.S., et al., *Detection of DNA hybridization using the near-infrared band-gap fluorescence of single-walled carbon nanotubes.* Nano letters, 2006. **6**(3): p. 371-375.
5. Iverson, N.M., et al., *In vivo biosensing via tissue-localizable near-infrared-fluorescent single-walled carbon nanotubes.* Nature nanotechnology, 2013. **8**(11): p. 873.
6. Harvey, J.D., et al., *A carbon nanotube reporter of microRNA hybridization events in vivo.* Nature biomedical engineering, 2017. **1**(4): p. 0041.
7. Zhang, J., et al., *A rapid, direct, quantitative, and label-free detector of cardiac biomarker troponin T using near-infrared fluorescent single-walled carbon nanotube sensors.* Advanced healthcare materials, 2014. **3**(3): p. 412-423.
8. Landry, M.P., et al., *Single-molecule detection of protein efflux from microorganisms using fluorescent single-walled carbon nanotube sensor arrays.* Nature nanotechnology, 2017. **12**(4): p. 368.
9. Zhang, J., et al., *Single molecule detection of nitric oxide enabled by d (AT) 15 DNA adsorbed to near infrared fluorescent single-walled carbon nanotubes.* Journal of the American Chemical Society, 2010. **133**(3): p. 567-581.
10. Kim, J.-H., et al., *Single-molecule detection of H2O2 mediating angiogenic redox signaling on fluorescent single-walled carbon nanotube array.* Acs Nano, 2011. **5**(10): p. 7848-7857.
11. Nimse, S.B., et al., *Immobilization techniques for microarray: challenges and applications.* Sensors, 2014. **14**(12): p. 22208-22229.
12. Green, N., *Avidin. 3. The nature of the biotin-binding site.* Biochemical Journal, 1963. **89**(3): p. 599.
13. Pon, R.T., *A long chain biotin phosphoramidite reagent for the automated synthesis of 5'-biotinylated oligonucleotides.* Tetrahedron letters, 1991. **32**(14): p. 1715-1718.
14. Cook, A.F., E. Vuocolo, and C.L. Brakel, *Synthesis and hybridization of a series of biotinylated oligonucleotides.* Nucleic acids research, 1988. **16**(9): p. 4077-4095.
15. Schena, M., *Protein microarrays*. 2005: Jones & Bartlett Learning.
16. Chen, K., R.N. Pittman, and A.S. Popel, *Nitric oxide in the vasculature: where does it come from and where does it go? A quantitative perspective.* Antioxidants & redox signaling, 2008. **10**(7): p. 1185-1198.

17. Calabrese, V., et al., *Nitric oxide in the central nervous system: neuroprotection versus neurotoxicity.* Nature Reviews Neuroscience, 2007. **8**(10): p. 766.
18. Wink, D.A., et al., *Nitric oxide and redox mechanisms in the immune response.* Journal of leukocyte biology, 2011. **89**(6): p. 873-891.
19. Cui, S., et al., *Activated murine macrophages induce apoptosis in tumor cells through nitric oxide-dependent or-independent mechanisms.* Cancer Research, 1994. **54**(9): p. 2462-2467.
20. Brüne, B., A. von Knethen, and K.B. Sandau, *Nitric oxide (NO): an effector of apoptosis.* Cell death and differentiation, 1999. **6**(10): p. 969.
21. Vannini, F., K. Kashfi, and N. Nath, *The dual role of iNOS in cancer.* Redox biology, 2015. **6**: p. 334-343.
22. Burke, A.J., et al., *The yin and yang of nitric oxide in cancer progression.* Carcinogenesis, 2013. **34**(3): p. 503-512.
23. Janakiram, N.B. and C.V. Rao, *iNOS-selective inhibitors for cancer prevention: promise and progress.* Future medicinal chemistry, 2012. **4**(17): p. 2193-2204.
24. Kashfi, K. and F. Vannini, *Nitric Oxide and Cancer: To Inhibit or To Induce iNOS: That Is the Question?*, in *Therapeutic Application of Nitric Oxide in Cancer and Inflammatory Disorders*. 2019, Elsevier. p. 93-111.
25. McCartney-Francis, N., et al., *Suppression of arthritis by an inhibitor of nitric oxide synthase.* Journal of Experimental Medicine, 1993. **178**(2): p. 749-754.
26. Mateen, S., et al., *Increased reactive oxygen species formation and oxidative stress in rheumatoid arthritis.* PloS one, 2016. **11**(4): p. e0152925.
27. Heydarpour, P., et al., *Behavioral despair associated with a mouse model of Crohn's disease: Role of nitric oxide pathway.* Progress in Neuro-Psychopharmacology and Biological Psychiatry, 2016. **64**: p. 131-141.
28. Boughton-Smith, N., et al., *Nitric oxide synthase activity in ulcerative colitis and Crohn's disease.* The Lancet, 1993. **342**(8867): p. 338-e2.
29. Tufvesson, E., et al., *Inducible nitric oxide synthase expression is increased in the alveolar compartment of asthmatic patients.* Allergy, 2017. **72**(4): p. 627-635.
30. Kharitonov, S., et al., *Increased nitric oxide in exhaled air of asthmatic patients.* The Lancet, 1994. **343**(8890): p. 133-135.
31. Balez, R. and L. Ooi, *Getting to NO Alzheimer's disease: neuroprotection versus neurotoxicity mediated by nitric oxide.* Oxidative medicine and cellular longevity, 2016. **2016**.
32. Chakroborty, S., et al., *Nitric oxide signaling is recruited as a compensatory mechanism for sustaining synaptic plasticity in Alzheimer's disease mice.* Journal of Neuroscience, 2015. **35**(17): p. 6893-6902.
33. Ayton, S., et al., *Parkinson's disease iron deposition caused by nitric oxide-induced loss of β-amyloid precursor protein.* Journal of Neuroscience, 2015. **35**(8): p. 3591-3597.
34. Zhang, L., V.L. Dawson, and T.M. Dawson, *Role of nitric oxide in Parkinson's disease.* Pharmacology & therapeutics, 2006. **109**(1-2): p. 33-41.
35. Yuste, J.E., et al., *Implications of glial nitric oxide in neurodegenerative diseases.* Frontiers in cellular neuroscience, 2015. **9**: p. 322.

36. Stokes, K.Y., et al., *Hypercholesterolemia promotes inflammation and microvascular dysfunction: role of nitric oxide and superoxide.* Free Radical Biology and Medicine, 2002. **33**(8): p. 1026-1036.
37. Feron, O., et al., *Hypercholesterolemia decreases nitric oxide production by promoting the interaction of caveolin and endothelial nitric oxide synthase.* The Journal of clinical investigation, 1999. **103**(6): p. 897-905.
38. Napoli, C. and L.J. Ignarro, *Nitric oxide and atherosclerosis.* Nitric oxide, 2001. **5**(2): p. 88-97.
39. Santilli, F., et al., *The role of nitric oxide in the development of diabetic angiopathy.* Hormone and metabolic research, 2004. **36**(05): p. 319-335.
40. Huang, P.L., et al., *Hypertension in mice lacking the gene for endothelial nitric oxide synthase.* Nature, 1995. **377**(6546): p. 239.
41. Landmesser, U., et al., *Oxidation of tetrahydrobiopterin leads to uncoupling of endothelial cell nitric oxide synthase in hypertension.* The Journal of clinical investigation, 2003. **111**(8): p. 1201-1209.
42. Khan, M., et al., *Cerebrovascular protection by various nitric oxide donors in rats after experimental stroke.* Nitric oxide, 2006. **15**(2): p. 114-124.
43. El Kossi, M.M.H. and M.M. Zakhary, *Oxidative stress in the context of acute cerebrovascular stroke.* Stroke, 2000. **31**(8): p. 1889-1892.
44. Li, H. and U. Förstermann, *Nitric oxide in the pathogenesis of vascular disease.* The Journal of pathology, 2000. **190**(3): p. 244-254.
45. Streit, J.K., et al., *Measuring single-walled carbon nanotube length distributions from diffusional trajectories.* Acs Nano, 2012. **6**(9): p. 8424-8431.
46. Nanot, S., et al., *Single-Walled Carbon Nanotubes*, in *Springer Handbook of Nanomaterials*. 2013, Springer. p. 105-146.
47. Zhu, H., et al., *Direct synthesis of long single-walled carbon nanotube strands.* Science, 2002. **296**(5569): p. 884-886.
48. Zheng, L., et al., *Ultralong single-wall carbon nanotubes.* Nature materials, 2004. **3**(10): p. 673.
49. Yu, M.-F., et al., *Tensile loading of ropes of single wall carbon nanotubes and their mechanical properties.* Physical review letters, 2000. **84**(24): p. 5552.
50. Cornwell, C. and L. Wille, *Elastic properties of single-walled carbon nanotubes in compression.* Solid State Communications, 1997. **101**(8): p. 555-558.
51. Falvo, M.R., et al., *Bending and buckling of carbon nanotubes under large strain.* Nature, 1997. **389**(6651): p. 582.
52. Hosseini, M., et al., *Size-dependent stress analysis of single-wall carbon nanotube based on strain gradient theory.* International Journal of Applied Mechanics, 2017. **9**(06): p. 1750087.
53. Yao, Z., C.L. Kane, and C. Dekker, *High-field electrical transport in single-wall carbon nanotubes.* Physical Review Letters, 2000. **84**(13): p. 2941.
54. Moisala, A., et al., *Thermal and electrical conductivity of single-and multi-walled carbon nanotube-epoxy composites.* Composites science and technology, 2006. **66**(10): p. 1285-1288.
55. Hone, J., et al., *Thermal conductivity of single-walled carbon nanotubes.* Physical Review B, 1999. **59**(4): p. R2514.

56. Arani, A.A.A., et al., *Heat transfer improvement of water/single-wall carbon nanotubes (SWCNT) nanofluid in a novel design of a truncated double-layered microchannel heat sink.* International Journal of Heat and Mass Transfer, 2017. **113**: p. 780-795.
57. Moser, M.L., et al., *Fast electrochromic device based on single-walled carbon nanotube thin films.* Nano letters, 2016. **16**(9): p. 5386-5393.
58. Li, F., et al., *Tensile strength of single-walled carbon nanotubes directly measured from their macroscopic ropes.* Applied physics letters, 2000. **77**(20): p. 3161-3163.
59. Meo, M. and M. Rossi, *Prediction of Young's modulus of single wall carbon nanotubes by molecular-mechanics based finite element modelling.* Composites Science and Technology, 2006. **66**(11-12): p. 1597-1605.
60. Salvetat, J.-P., et al., *Elastic and shear moduli of single-walled carbon nanotube ropes.* Physical review letters, 1999. **82**(5): p. 944.
61. Guthy, C., et al., *Thermal conductivity of single-walled carbon nanotube/PMMA nanocomposites.* Journal of heat transfer, 2007. **129**(8): p. 1096-1099.
62. Berber, S., Y.-K. Kwon, and D. Tománek, *Unusually high thermal conductivity of carbon nanotubes.* Physical review letters, 2000. **84**(20): p. 4613.
63. Harrison, B.S. and A. Atala, *Carbon nanotube applications for tissue engineering.* Biomaterials, 2007. **28**(2): p. 344-353.
64. Gul, H., et al., *Magnetic carbon nanotube labelling for haematopoietic stem/progenitor cell tracking.* Nanotechnology, 2010. **21**(15): p. 155101.
65. Lamanna, G., et al., *Endowing carbon nanotubes with superparamagnetic properties: applications for cell labeling, MRI cell tracking and magnetic manipulations.* Nanoscale, 2013. **5**(10): p. 4412-4421.
66. Liu, Z., et al., *siRNA delivery into human T cells and primary cells with carbon-nanotube transporters.* Angewandte Chemie International Edition, 2007. **46**(12): p. 2023-2027.
67. Kruss, S., et al., *Carbon nanotubes as optical biomedical sensors.* Advanced drug delivery reviews, 2013. **65**(15): p. 1933-1950.
68. Correa-Duarte, M.A., et al., *Fabrication and biocompatibility of carbon nanotube-based 3D networks as scaffolds for cell seeding and growth.* Nano Letters, 2004. **4**(11): p. 2233-2236.
69. Ulissi, Z.W., et al., *Spatiotemporal intracellular nitric oxide signaling captured using internalized, near-infrared fluorescent carbon nanotube nanosensors.* Nano letters, 2014. **14**(8): p. 4887-4894.
70. Barone, P.W., R.S. Parker, and M.S. Strano, *In vivo fluorescence detection of glucose using a single-walled carbon nanotube optical sensor: design, fluorophore properties, advantages, and disadvantages.* Analytical chemistry, 2005. **77**(23): p. 7556-7562.
71. Jin, H., et al., *Detection of single-molecule H 2 O 2 signalling from epidermal growth factor receptor using fluorescent single-walled carbon nanotubes.* Nature Nanotechnology, 2010. **5**(4): p. 302.
72. Heller, D.A., et al., *Optical detection of DNA conformational polymorphism on single-walled carbon nanotubes.* Science, 2006. **311**(5760): p. 508-511.

73. Kruss, S., et al., *High-resolution imaging of cellular dopamine efflux using a fluorescent nanosensor array.* Proceedings of the National Academy of Sciences, 2017. **114**(8): p. 1789-1794.
74. Dong, J., et al., *Analysis of multiplexed nanosensor arrays based on near-infrared fluorescent single-walled carbon nanotubes.* ACS nano, 2018. **12**(4): p. 3769-3779.
75. Satishkumar, B., et al., *Reversible fluorescence quenching in carbon nanotubes for biomolecular sensing.* Nature Nanotechnology, 2007. **2**(9): p. 560.
76. So, H.-M., et al., *Single-walled carbon nanotube biosensors using aptamers as molecular recognition elements.* Journal of the American Chemical Society, 2005. **127**(34): p. 11906-11907.
77. Bisker, G., et al., *Insulin detection using a corona phase molecular recognition site on single-walled carbon nanotubes.* ACS sensors, 2018. **3**(2): p. 367-377.
78. Zhang, J., et al., *Molecular recognition using nanotube-adsorbed polymer phases: nanotube antibodies.* Nature nanotechnology, 2013. **8**(12): p. 959.
79. Kim, J.-H., et al., *The rational design of nitric oxide selectivity in single-walled carbon nanotube near-infrared fluorescence sensors for biological detection.* Nature Chemistry, 2009. **1**(6): p. 473.
80. Galassi, T.V., et al., *An optical nanoreporter of endolysosomal lipid accumulation reveals enduring effects of diet on hepatic macrophages in vivo.* Science translational medicine, 2018. **10**(461): p. eaar2680.
81. Kim, J.H., et al., *A luciferase/single-walled carbon nanotube conjugate for near-infrared fluorescent detection of cellular ATP.* Angewandte Chemie International Edition, 2010. **49**(8): p. 1456-1459.
82. Jin, H., et al., *Divalent ion and thermally induced DNA conformational polymorphism on single-walled carbon nanotubes.* Macromolecules, 2007. **40**(18): p. 6731-6739.
83. Jeong, S., et al., *High Throughput Evolution of Near Infrared Serotonin Nanosensors.* bioRxiv, 2019: p. 673152.
84. Beyene, A.G., et al., *Imaging striatal dopamine release using a nongenetically encoded near infrared fluorescent catecholamine nanosensor.* Science advances, 2019. **5**(7): p. eaaw3108.
85. Borland, C., *Endothelium in control.* British heart journal, 1991. **66**(5): p. 405.
86. Liu, X., et al., *Diffusion-limited reaction of free nitric oxide with erythrocytes.* Journal of biological chemistry, 1998. **273**(30): p. 18709-18713.
87. Vaughn, M.W., et al., *Erythrocytes possess an intrinsic barrier to nitric oxide consumption.* Journal of Biological Chemistry, 2000. **275**(4): p. 2342-2348.
88. Rassaf, T., et al., *Evidence for in vivo transport of bioactive nitric oxide in human plasma.* The Journal of clinical investigation, 2002. **109**(9): p. 1241-1248.
89. Wagner, B.A., et al., *An assay for the rate of removal of extracellular hydrogen peroxide by cells.* Redox biology, 2013. **1**(1): p. 210-217.
90. Journet, C., et al., *Large-scale production of single-walled carbon nanotubes by the electric-arc technique.* Nature, 1997. **388**(6644): p. 756.
91. Smalley, R.E. and R.E. Haufler, *Electric arc process for making fullerenes*. 1993, Google Patents.

92. De La Chapelle, M.L., et al., *Raman studies on single walled carbon nanotubes produced by the electric arc technique.* Carbon, 1998. **36**(5-6): p. 705-708.
93. Itkis, M., et al., *Optimization of the Ni− Y catalyst composition in bulk electric arc synthesis of single-walled carbon nanotubes by use of near-infrared spectroscopy.* The Journal of Physical Chemistry B, 2004. **108**(34): p. 12770-12775.
94. Mathur, R., et al., *Co-synthesis, purification and characterization of single-and multi-walled carbon nanotubes using the electric arc method.* Carbon, 2007. **45**(1): p. 132-140.
95. Fiorito, S., *Carbon nanotubes: angels or demons?* 2019: CRC Press.
96. Kim, K.S., et al., *Large-scale production of single-walled carbon nanotubes by induction thermal plasma.* Journal of physics D: Applied physics, 2007. **40**(8): p. 2375.
97. Yu, A., et al., *Application of centrifugation to the large-scale purification of electric arc-produced single-walled carbon nanotubes.* Journal of the American Chemical Society, 2006. **128**(30): p. 9902-9908.
98. Yudasaka, M., et al., *Single-wall carbon nanotube formation by laser ablation using double-targets of carbon and metal.* Chemical physics letters, 1997. **278**(1-3): p. 102-106.
99. Maser, W., et al., *Production of high-density single-walled nanotube material by a simple laser-ablation method.* Chemical Physics Letters, 1998. **292**(4-6): p. 587-593.
100. Kingston, C.T., et al., *Efficient laser synthesis of single-walled carbon nanotubes through laser heating of the condensing vaporization plume.* Carbon, 2004. **42**(8-9): p. 1657-1664.
101. Yudasaka, M., et al., *Mechanism of the effect of NiCo, Ni and Co catalysts on the yield of single-wall carbon nanotubes formed by pulsed Nd: YAG laser ablation.* The Journal of Physical Chemistry B, 1999. **103**(30): p. 6224-6229.
102. Kokai, F., et al., *Growth dynamics of single-wall carbon nanotubes synthesized by CO2 laser vaporization.* The Journal of Physical Chemistry B, 1999. **103**(21): p. 4346-4351.
103. Kataura, H., et al., *Diameter control of single-walled carbon nanotubes.* Carbon, 2000. **38**(11-12): p. 1691-1697.
104. Colomer, J.-F., et al., *Large-scale synthesis of single-wall carbon nanotubes by catalytic chemical vapor deposition (CCVD) method.* Chemical Physics Letters, 2000. **317**(1-2): p. 83-89.
105. Colomer, J.-F., et al., *Characterization of single-wall carbon nanotubes produced by CCVD method.* Chemical Physics Letters, 2001. **345**(1-2): p. 11-17.
106. Tang, S., et al., *Controlled growth of single-walled carbon nanotubes by catalytic decomposition of CH4 over Mo/Co/MgO catalysts.* Chemical Physics Letters, 2001. **350**(1-2): p. 19-26.
107. Maruyama, S., et al., *Low-temperature synthesis of high-purity single-walled carbon nanotubes from alcohol.* Chemical physics letters, 2002. **360**(3-4): p. 229-234.

108. Kong, J., A.M. Cassell, and H. Dai, *Chemical vapor deposition of methane for single-walled carbon nanotubes.* Chemical physics letters, 1998. **292**(4-6): p. 567-574.
109. Zhang, R.Y., et al., *Chemical vapor deposition of single-walled carbon nanotubes using ultrathin Ni/Al film as catalyst.* Nano Letters, 2003. **3**(6): p. 731-735.
110. Delzeit, L., et al., *Growth of carbon nanotubes by thermal and plasma chemical vapour deposition processes and applications in microscopy.* Nanotechnology, 2002. **13**(3): p. 280.
111. Dai, H., et al., *Single-wall nanotubes produced by metal-catalyzed disproportionation of carbon monoxide.* Chemical physics letters, 1996. **260**(3-4): p. 471-475.
112. Hafner, J.H., et al., *Catalytic growth of single-wall carbon nanotubes from metal particles.* Chemical Physics Letters, 1998. **296**(1-2): p. 195-202.
113. Nikolaev, P., et al., *Gas-phase catalytic growth of single-walled carbon nanotubes from carbon monoxide.* Chemical physics letters, 1999. **313**(1-2): p. 91-97.
114. Bronikowski, M.J., et al., *Gas-phase production of carbon single-walled nanotubes from carbon monoxide via the HiPco process: A parametric study.* Journal of Vacuum Science & Technology A: Vacuum, Surfaces, and Films, 2001. **19**(4): p. 1800-1805.
115. Flahaut, E., et al., *Synthesis of single-walled carbon nanotubes using binary (Fe, Co, Ni) alloy nanoparticles prepared in situ by the reduction of oxide solid solutions.* Chemical Physics Letters, 1999. **300**(1-2): p. 236-242.
116. Hafner, J.H., et al., *High-yield assembly of individual single-walled carbon nanotube tips for scanning probe microscopies.* The Journal of Physical Chemistry B, 2001. **105**(4): p. 743-746.
117. Satishkumar, B., et al., *Single-walled nanotubes by the pyrolysis of acetylene-organometallic mixtures.* Chemical Physics Letters, 1998. **293**(1-2): p. 47-52.
118. Cheng, H., et al., *Bulk morphology and diameter distribution of single-walled carbon nanotubes synthesized by catalytic decomposition of hydrocarbons.* Chemical Physics Letters, 1998. **289**(5-6): p. 602-610.
119. Chen, Y. and J. Zhang, *Chemical vapor deposition growth of single-walled carbon nanotubes with controlled structures for nanodevice applications.* Accounts of chemical research, 2014. **47**(8): p. 2273-2281.
120. Sen, R., A. Govindaraj, and C. Rao, *Metal-filled and hollow carbon nanotubes obtained by the decomposition of metal-containing free precursor molecules.* Chemistry of Materials, 1997. **9**(10): p. 2078-2081.
121. Bachilo, S.M., et al., *Structure-assigned optical spectra of single-walled carbon nanotubes.* Science, 2002. **298**(5602): p. 2361-2366.
122. O'connell, M.J., et al., *Band gap fluorescence from individual single-walled carbon nanotubes.* Science, 2002. **297**(5581): p. 593-596.
123. Matsuda, Y., J. Tahir-Kheli, and W.A. Goddard III, *Definitive band gaps for single-wall carbon nanotubes.* The Journal of Physical Chemistry Letters, 2010. **1**(19): p. 2946-2950.
124. Strano, M.S., et al., *Electronic structure control of single-walled carbon nanotube functionalization.* Science, 2003. **301**(5639): p. 1519-1522.

125. Thess, A., et al., *Crystalline ropes of metallic carbon nanotubes.* Science, 1996. **273**(5274): p. 483-487.
126. Girifalco, L., M. Hodak, and R.S. Lee, *Carbon nanotubes, buckyballs, ropes, and a universal graphitic potential.* Physical Review B, 2000. **62**(19): p. 13104.
127. Dresselhaus, G. and S. Riichiro, *Physical properties of carbon nanotubes*. 1998: World scientific.
128. Saito, R., G. Dresselhaus, and M. Dresselhaus, *Trigonal warping effect of carbon nanotubes.* Physical Review B, 2000. **61**(4): p. 2981.
129. Stolik, S., et al., *Measurement of the penetration depths of red and near infrared light in human "ex vivo" tissues.* Journal of Photochemistry and Photobiology B: Biology, 2000. **57**(2-3): p. 90-93.
130. Welsher, K., S.P. Sherlock, and H. Dai, *Deep-tissue anatomical imaging of mice using carbon nanotube fluorophores in the second near-infrared window.* Proceedings of the National Academy of Sciences, 2011. **108**(22): p. 8943-8948.
131. Frangioni, J.V., *In vivo near-infrared fluorescence imaging.* Current opinion in chemical biology, 2003. **7**(5): p. 626-634.
132. Kim, B.C., et al., *Fabrication of enzyme-based coatings on intact multi-walled carbon nanotubes as highly effective electrodes in biofuel cells.* Scientific reports, 2017. **7**: p. 40202.
133. Heller, D.A., et al., *Multimodal optical sensing and analyte specificity using single-walled carbon nanotubes.* Nature Nanotechnology, 2009. **4**(2): p. 114.
134. Bahr, J.L. and J.M. Tour, *Covalent chemistry of single-wall carbon nanotubes.* Journal of Materials Chemistry, 2002. **12**(7): p. 1952-1958.
135. Moore, V.C., et al., *Individually suspended single-walled carbon nanotubes in various surfactants.* Nano letters, 2003. **3**(10): p. 1379-1382.
136. Zheng, M., et al., *DNA-assisted dispersion and separation of carbon nanotubes.* Nature materials, 2003. **2**(5): p. 338.
137. Strano, M.S., et al., *The role of surfactant adsorption during ultrasonication in the dispersion of single-walled carbon nanotubes.* Journal of nanoscience and nanotechnology, 2003. **3**(1-2): p. 81-86.
138. Heller, D.A., et al., *Single-walled carbon nanotube spectroscopy in live cells: towards long-term labels and optical sensors.* Advanced Materials, 2005. **17**(23): p. 2793-2799.
139. Blum, C., et al., *Selective bundling of zigzag single-walled carbon nanotubes.* ACS nano, 2011. **5**(4): p. 2847-2854.
140. Bao, P., et al., *High-sensitivity detection of DNA hybridization on microarrays using resonance light scattering.* Analytical chemistry, 2002. **74**(8): p. 1792-1797.
141. Li, Y., Y.T.H. Cu, and D. Luo, *Multiplexed detection of pathogen DNA with DNA-based fluorescence nanobarcodes.* Nature biotechnology, 2005. **23**(7): p. 885.
142. Louws, F.J., et al., *Specific genomic fingerprints of phytopathogenic Xanthomonas and Pseudomonas pathovars and strains generated with repetitive sequences and PCR.* Appl. Environ. Microbiol., 1994. **60**(7): p. 2286-2295.
143. Schork, N.J., D. Fallin, and J.S. Lanchbury, *Single nucleotide polymorphisms and the future of genetic epidemiology.* Clinical genetics, 2000. **58**(4): p. 250-264.

144. Wang, D.G., et al., *Large-scale identification, mapping, and genotyping of single-nucleotide polymorphisms in the human genome.* Science, 1998. **280**(5366): p. 1077-1082.
145. McCarthy, J.J. and R. Hilfiker, *The use of single-nucleotide polymorphism maps in pharmacogenomics.* Nature biotechnology, 2000. **18**(5): p. 505.
146. Cooper, D.S., et al., *L-thyroxine therapy in subclinical hypothyroidism: a double-blind, placebo-controlled trial.* Annals of internal medicine, 1984. **101**(1): p. 18-24.
147. Darbre, P., et al., *Effect of estradiol on human breast cancer cells in culture.* Cancer Research, 1983. **43**(1): p. 349-354.
148. Barone, P.W., et al., *Near-infrared optical sensors based on single-walled carbon nanotubes.* Nature materials, 2005. **4**(1): p. 86.
149. Cognet, L., et al., *Stepwise quenching of exciton fluorescence in carbon nanotubes by single-molecule reactions.* Science, 2007. **316**(5830): p. 1465-1468.
150. Zhao, C., et al., *A Reusable DNA Single-Walled Carbon-Nanotube-Based Fluorescent Sensor for Highly Sensitive and Selective Detection of Ag+ and Cysteine in Aqueous Solutions.* Chemistry–A European Journal, 2010. **16**(27): p. 8147-8154.
151. Harvey, J.D., et al., *An in Vivo Nanosensor Measures Compartmental Doxorubicin Exposure.* Nano Letters, 2019.
152. Bieghs, V., et al., *Trapping of oxidized LDL in lysosomes of K upffer cells is a trigger for hepatic inflammation.* Liver International, 2013. **33**(7): p. 1056-1061.
153. Nixon, R.A., *The role of autophagy in neurodegenerative disease.* Nature medicine, 2013. **19**(8): p. 983.
154. Kirkegaard, T. and M. Jäättelä, *Lysosomal involvement in cell death and cancer.* Biochimica et Biophysica Acta (BBA)-Molecular Cell Research, 2009. **1793**(4): p. 746-754.
155. Welsher, K., et al., *Selective probing and imaging of cells with single walled carbon nanotubes as near-infrared fluorescent molecules.* Nano letters, 2008. **8**(2): p. 586-590.
156. Eccles, S.A., *The role of c-erbB-2/HER2/neu in breast cancer progression and metastasis.* Journal of mammary gland biology and neoplasia, 2001. **6**(4): p. 393-406.
157. Bareford, L.M., et al., *Intracellular processing of riboflavin in human breast cancer cells.* Molecular pharmaceutics, 2008. **5**(5): p. 839-848.
158. Bhattacharya, S., et al., *DNA conjugated SWCNTs enter endothelial cells via Rac1 mediated macropinocytosis.* Nano letters, 2012. **12**(4): p. 1826-1830.
159. Jin, H., D.A. Heller, and M.S. Strano, *Single-particle tracking of endocytosis and exocytosis of single-walled carbon nanotubes in NIH-3T3 cells.* Nano letters, 2008. **8**(6): p. 1577-1585.
160. Bickerstaff, G.F., *Immobilization of enzymes and cells*, in *Immobilization of enzymes and cells*. 1997, Springer. p. 1-11.
161. Kim, D. and A.E. Herr, *Protein immobilization techniques for microfluidic assays.* Biomicrofluidics, 2013. **7**(4): p. 041501.

162. Mann, F.A., et al., *Nanobody-Conjugated Nanotubes for Targeted Near-Infrared In Vivo Imaging and Sensing.* Angewandte Chemie International Edition, 2019. **58**(33): p. 11469-11473.
163. Lee, M.A., et al., *Implanted Nanosensors in Marine Organisms for Physiological Biologging: Design, Feasibility, and Species Variability.* ACS sensors, 2018. **4**(1): p. 32-43.
164. Zhang, Y., et al., *Cytotoxicity effects of graphene and single-wall carbon nanotubes in neural phaeochromocytoma-derived PC12 cells.* ACS nano, 2010. **4**(6): p. 3181-3186.
165. Tian, F., et al., *Cytotoxicity of single-wall carbon nanotubes on human fibroblasts.* Toxicology in vitro, 2006. **20**(7): p. 1202-1212.
166. Shvedova, A., et al., *Exposure to carbon nanotube material: assessment of nanotube cytotoxicity using human keratinocyte cells.* Journal of toxicology and environmental health Part A, 2003. **66**(20): p. 1909-1926.
167. Casey, A., et al., *Spectroscopic analysis confirms the interactions between single walled carbon nanotubes and various dyes commonly used to assess cytotoxicity.* Carbon, 2007. **45**(7): p. 1425-1432.
168. Wörle-Knirsch, J., K. Pulskamp, and H. Krug, *Oops they did it again! Carbon nanotubes hoax scientists in viability assays.* Nano letters, 2006. **6**(6): p. 1261-1268.
169. Belyanskaya, L., et al., *The reliability and limits of the MTT reduction assay for carbon nanotubes–cell interaction.* Carbon, 2007. **45**(13): p. 2643-2648.
170. Cui, D., et al., *Effect of single wall carbon nanotubes on human HEK293 cells.* Toxicology letters, 2005. **155**(1): p. 73-85.
171. Davoren, M., et al., *In vitro toxicity evaluation of single walled carbon nanotubes on human A549 lung cells.* Toxicology in vitro, 2007. **21**(3): p. 438-448.
172. Budhathoki-Uprety, J., et al., *A carbon nanotube optical sensor reports nuclear entry via a noncanonical pathway.* ACS nano, 2017. **11**(4): p. 3875-3882.
173. Becker, M.L., et al., *Length-dependent uptake of DNA-wrapped single-walled carbon nanotubes.* Advanced Materials, 2007. **19**(7): p. 939-945.
174. Gao, Z., et al., *Toward the suppression of cellular toxicity from single-walled carbon nanotubes.* Biomaterials science, 2016. **4**(2): p. 230-244.
175. Liu, Z., et al., *Circulation and long-term fate of functionalized, biocompatible single-walled carbon nanotubes in mice probed by Raman spectroscopy.* Proceedings of the National Academy of Sciences, 2008. **105**(5): p. 1410-1415.
176. Liu, Z., et al., *Carbon nanotubes in biology and medicine: in vitro and in vivo detection, imaging and drug delivery.* Nano research, 2009. **2**(2): p. 85-120.
177. Liu, Z., et al., *Preparation of carbon nanotube bioconjugates for biomedical applications.* Nature protocols, 2009. **4**(9): p. 1372.
178. Welsher, K., et al., *A route to brightly fluorescent carbon nanotubes for near-infrared imaging in mice.* Nature nanotechnology, 2009. **4**(11): p. 773.
179. Leeuw, T.K., et al., *Single-walled carbon nanotubes in the intact organism: near-IR imaging and biocompatibility studies in Drosophila.* Nano letters, 2007. **7**(9): p. 2650-2654.

180. Ahn, J.-H., et al., *Label-free, single protein detection on a near-infrared fluorescent single-walled carbon nanotube/protein microarray fabricated by cell-free synthesis.* Nano letters, 2011. **11**(7): p. 2743-2752.
181. Landry, M.P., et al., *Comparative dynamics and sequence dependence of DNA and RNA binding to single walled carbon nanotubes.* The Journal of Physical Chemistry C, 2015. **119**(18): p. 10048-10058.
182. Ratner, B.D. and A.S. Hoffman, *CHAPTER I. 2.12 PHYSICOCHEMICAL SURFACE MODIFICATION OF MATERIALS USED IN MEDICINE.* Biomaterials science: An introduction to materials in medicine, 2012: p. 259.
183. Lavoie, G.A., J.B. Heywood, and J.C. Keck, *Experimental and theoretical study of nitric oxide formation in internal combustion engines.* Combustion science and technology, 1970. **1**(4): p. 313-326.
184. Yetik-Anacak, G. and J.D. Catravas, *Nitric oxide and the endothelium: history and impact on cardiovascular disease.* Vascular pharmacology, 2006. **45**(5): p. 268-276.
185. Cech, T.R., et al., *The molecule of the year.* Science, 1992. **258**(1861).
186. Brown, J.F., P.J. Hanson, and B.J. Whittle, *Nitric oxide donors increase mucus gel thickness in rat stomach.* European journal of pharmacology, 1992. **223**(1): p. 103-104.
187. Brown, J., et al., *Nitric oxide generators and cGMP stimulate mucus secretion by rat gastric mucosal cells.* American Journal of Physiology-Gastrointestinal and Liver Physiology, 1993. **265**(3): p. G418-G422.
188. Lanas, A., *Role of nitric oxide in the gastrointestinal tract.* Arthritis Research & Therapy, 2008. **10**(2): p. S4.
189. Furukawa, O., et al., *Stimulatory effect of nitric oxide on bicarbonate secretion in bullfrog duodenums in vitro.* Digestion, 1999. **60**(4): p. 324-331.
190. Kato, S., et al., *Role of nitric oxide in regulation of gastric acid secretion in rats: effects of NO donors and NO synthase inhibitor.* British journal of pharmacology, 1998. **123**(5): p. 839-846.
191. Chen, S.-R., X.-G. Jin, and H.-L. Pan, *Endogenous nitric oxide inhibits spinal NMDA receptor activity and pain hypersensitivity induced by nerve injury.* Neuropharmacology, 2017. **125**: p. 156-165.
192. Cury, Y., et al., *Pain and analgesia: the dual effect of nitric oxide in the nociceptive system.* Nitric oxide, 2011. **25**(3): p. 243-254.
193. Gaskin, F.S., et al., *Ghrelin-induced feeding is dependent on nitric oxide.* Peptides, 2003. **24**(6): p. 913-918.
194. Kapás, L., J. Fang, and J.M. Krueger, *Inhibition of nitric oxide synthesis inhibits rat sleep.* Brain research, 1994. **664**(1-2): p. 189-196.
195. Contestabile, A. and E. Ciani, *Role of nitric oxide in the regulation of neuronal proliferation, survival and differentiation.* Neurochemistry international, 2004. **45**(6): p. 903-914.
196. Melino, G., et al., *S-nitrosylation regulates apoptosis.* Nature, 1997. **388**(6641): p. 432.
197. Gu, Z., et al., *S-nitrosylation of matrix metalloproteinases: signaling pathway to neuronal cell death.* Science, 2002. **297**(5584): p. 1186-1190.

198. Yao, D., et al., *Nitrosative stress linked to sporadic Parkinson's disease: S-nitrosylation of parkin regulates its E3 ubiquitin ligase activity.* Proceedings of the National Academy of Sciences, 2004. **101**(29): p. 10810-10814.
199. Bogdan, C., *Nitric oxide and the immune response.* Nature immunology, 2001. **2**(10): p. 907.
200. Lorsbach, R.B., et al., *Expression of the nitric oxide synthase gene in mouse macrophages activated for tumor cell killing. Molecular basis for the synergy between interferon-gamma and lipopolysaccharide.* Journal of Biological Chemistry, 1993. **268**(3): p. 1908-1913.
201. Fang, F.C., *Perspectives series: host/pathogen interactions. Mechanisms of nitric oxide-related antimicrobial activity.* The Journal of clinical investigation, 1997. **99**(12): p. 2818-2825.
202. Nathan, C., *Inducible nitric oxide synthase: what difference does it make?* The Journal of clinical investigation, 1997. **100**(10): p. 2417-2423.
203. Förstermann, U. and W.C. Sessa, *Nitric oxide synthases: regulation and function.* European heart journal, 2011. **33**(7): p. 829-837.
204. Crane, B.R., et al., *Structure of nitric oxide synthase oxygenase dimer with pterin and substrate.* Science, 1998. **279**(5359): p. 2121-2126.
205. Zhou, L. and D.-Y. Zhu, *Neuronal nitric oxide synthase: structure, subcellular localization, regulation, and clinical implications.* Nitric oxide, 2009. **20**(4): p. 223-230.
206. MacDonald, M.E., et al., *The Huntington's disease candidate region exhibits many different haplotypes.* Nature genetics, 1992. **1**(2): p. 99.
207. Kelm, M., *Nitric oxide metabolism and breakdown.* Biochimica et Biophysica Acta (BBA)-Bioenergetics, 1999. **1411**(2-3): p. 273-289.
208. Griess, P., *Bemerkungen zu der Abhandlung der HH. Weselsky und Benedikt „Ueber einige Azoverbindungen"* . Berichte der deutschen chemischen Gesellschaft, 1879. **12**(1): p. 426-428.
209. Lundberg, J.O., E. Weitzberg, and M.T. Gladwin, *The nitrate–nitrite–nitric oxide pathway in physiology and therapeutics.* Nature reviews Drug discovery, 2008. **7**(2): p. 156.
210. Rassaf, T., P. Ferdinandy, and R. Schulz, *Nitrite in organ protection.* British journal of pharmacology, 2014. **171**(1): p. 1-11.
211. Csonka, C., et al., *Measurement of NO in biological samples.* British journal of pharmacology, 2015. **172**(6): p. 1620-1632.
212. Bredt, D.S. and S.H. Snyder, *Isolation of nitric oxide synthetase, a calmodulin-requiring enzyme.* Proceedings of the National Academy of Sciences, 1990. **87**(2): p. 682-685.
213. Iverson, N., E. Hofferber, and J. Stapleton, *Nitric Oxide Sensors for Biological Applications.* Chemosensors, 2018. **6**(1): p. 8.
214. Kojima, H., et al., *Fluorescent indicators for imaging nitric oxide production.* Angewandte Chemie International Edition, 1999. **38**(21): p. 3209-3212.
215. Zhang, X., et al., *Interfering with nitric oxide measurements 4, 5-diaminofluorescein reacts with dehydroascorbic acid and ascorbic acid.* Journal of Biological Chemistry, 2002. **277**(50): p. 48472-48478.

216. Kojima, H., et al., *Bioimaging of nitric oxide with fluorescent indicators based on the rhodamine chromophore.* Analytical chemistry, 2001. **73**(9): p. 1967-1973.
217. Ye, X., S.S. Rubakhin, and J.V. Sweedler, *Simultaneous nitric oxide and dehydroascorbic acid imaging by combining diaminofluoresceins and diaminorhodamines.* Journal of neuroscience methods, 2008. **168**(2): p. 373-382.
218. Radi, R., *Reactions of nitric oxide with metalloproteins.* Chemical research in toxicology, 1996. **9**(5): p. 828-835.
219. Lim, M.H. and S.J. Lippard, *Metal-based turn-on fluorescent probes for sensing nitric oxide.* Accounts of chemical research, 2007. **40**(1): p. 41-51.
220. Hilderbrand, S.A., M.H. Lim, and S.J. Lippard, *Dirhodium tetracarboxylate scaffolds as reversible fluorescence-based nitric oxide sensors.* Journal of the American Chemical Society, 2004. **126**(15): p. 4972-4978.
221. Smith, R.C., et al., *Conjugated polymer-based fluorescence turn-on sensor for nitric oxide.* Organic letters, 2005. **7**(16): p. 3573-3575.
222. Chen, X., et al., *Fluorescent and luminescent probes for detection of reactive oxygen and nitrogen species.* Chemical Society Reviews, 2011. **40**(9): p. 4783-4804.
223. Wang, S., M.-Y. Han, and D. Huang, *Nitric oxide switches on the photoluminescence of molecularly engineered quantum dots.* Journal of the American Chemical Society, 2009. **131**(33): p. 11692-11694.
224. Yan, X.Q., et al., *Fluorescence sensing of nitric oxide in aqueous solution by triethanolamine-modified CdSe quantum dots.* Luminescence: The journal of biological and chemical luminescence, 2009. **24**(4): p. 255-259.
225. Myung, N., Y. Bae, and A.J. Bard, *Enhancement of the photoluminescence of CdSe nanocrystals dispersed in CHCl3 by oxygen passivation of surface states.* Nano letters, 2003. **3**(6): p. 747-749.
226. Shu, G.-W., et al., *Photoluminescence of colloidal CdSe/ZnS quantum dots under oxygen atmosphere.* IEEE Transactions on nanotechnology, 2005. **4**(5): p. 632-636.
227. Adegoke, O. and P.B. Forbes, *Challenges and advances in quantum dot fluorescent probes to detect reactive oxygen and nitrogen species: a review.* Analytica Chimica Acta, 2015. **862**: p. 1-13.
228. Weil, J.A. and J.R. Bolton, *Electron paramagnetic resonance: elementary theory and practical applications*. 2007: John Wiley & Sons.
229. Hogg, N., *Detection of nitric oxide by electron paramagnetic resonance spectroscopy.* Free Radical Biology and Medicine, 2010. **49**(2): p. 122-129.
230. Uehara, H. and S. Arimitsu, *Gas-phase electron paramagnetic resonance detection of nitric oxide and nitrogen dioxide in polluted air.* Analytical chemistry, 1973. **45**(11): p. 1897-1900.
231. Arroyo, C.M. and C. Forray, *Activation of cyclic GMP formation in mouse neuroblastoma cells by a labile nitroxyl radical. An electron paramagnetic resonance/spin trapping study.* European Journal of Pharmacology: Molecular Pharmacology, 1991. **208**(2): p. 157-161.
232. Arroyo, C.M. and M. Kohno, *Difficulties encountered in the detection of nitric oxide (NO) by spin trapping techniques. A cautionary note.* Free radical research communications, 1991. **14**(2): p. 145-155.

233. Korth, H.G., et al., *Tetramethyl-Ortho-quinodimethane, first member of a family of custom-tailored cheletropic spin traps for nitric oxide.* Angewandte Chemie International Edition in English, 1992. **31**(7): p. 891-893.
234. Katayama, Y., N. Soh, and M. Maeda, *A new strategy for the design of molecular probes for investigating endogenous nitric oxide using an EPR or fluorescent technique.* ChemPhysChem, 2001. **2**(11): p. 655-661.
235. Hawkins, C.L. and M.J. Davies, *Detection and characterisation of radicals in biological materials using EPR methodology.* Biochimica et Biophysica Acta (BBA)-General Subjects, 2014. **1840**(2): p. 708-721.
236. Greenberg, S.S., D.E. Wilcox, and G.M. Rubanyi, *Endothelium-derived relaxing factor released from canine femoral artery by acetylcholine cannot be identified as free nitric oxide by electron paramagnetic resonance spectroscopy.* Circulation research, 1990. **67**(6): p. 1446-1452.
237. Henry, Y., et al., *Nitric oxide, a biological effector.* European biophysics journal, 1991. **20**(1): p. 1-15.
238. Eriksson, L.G., *Binding of nitric oxide to intact human erythrocytes as monitored by electron paramagnetic resonance.* Biochemical and biophysical research communications, 1994. **203**(1): p. 176-181.
239. Piknova, B., et al., *Electron paramagnetic resonance analysis of nitrosylhemoglobin in humans during NO inhalation.* Journal of Biological Chemistry, 2005. **280**(49): p. 40583-40588.
240. Zhao, Y., et al., *A molecular basis for nitric oxide sensing by soluble guanylate cyclase.* Proceedings of the National Academy of Sciences, 1999. **96**(26): p. 14753-14758.
241. Woldman, Y.Y., et al., *Direct chemiluminescence detection of nitric oxide in aqueous solutions using the natural nitric oxide target soluble guanylyl cyclase.* Free Radical Biology and Medicine, 2009. **47**(10): p. 1339-1345.
242. Woldman, Y.Y., et al., *Detection of nitric oxide production in cell cultures by luciferin–luciferase chemiluminescence.* Biochemical and biophysical research communications, 2015. **465**(2): p. 232-238.
243. Schieber, M. and N.S. Chandel, *ROS function in redox signaling and oxidative stress.* Current biology, 2014. **24**(10): p. R453-R462.
244. Dinger, M.E., T.R. Mercer, and J.S. Mattick, *RNAs as extracellular signaling molecules.* Journal of molecular endocrinology, 2008. **40**(4): p. 151-159.
245. Fields, R.D. and B. Stevens, *ATP: an extracellular signaling molecule between neurons and glia.* Trends in neurosciences, 2000. **23**(12): p. 625-633.
246. Hankenson, K., K. Gagne, and M. Shaughnessy, *Extracellular signaling molecules to promote fracture healing and bone regeneration.* Advanced drug delivery reviews, 2015. **94**: p. 3-12.
247. Akamizu, T., et al., *Separate measurement of plasma levels of acylated and desacyl ghrelin in healthy subjects using a new direct ELISA assay.* The Journal of Clinical Endocrinology & Metabolism, 2005. **90**(1): p. 6-9.
248. Ida, N., et al., *Analysis of heterogeneous βA4 peptides in human cerebrospinal fluid and blood by a newly developed sensitive Western blot assay.* Journal of Biological Chemistry, 1996. **271**(37): p. 22908-22914.

249. Sinkala, E., et al., *Profiling protein expression in circulating tumour cells using microfluidic western blotting.* Nature communications, 2017. **8**: p. 14622.
250. Gelsinger, S., et al., *Comparison of radial immunodiffusion and ELISA for quantification of bovine immunoglobulin G in colostrum and plasma.* Journal of dairy science, 2015. **98**(6): p. 4084-4089.
251. Groseclose, M.R., et al., *Identification of proteins directly from tissue: in situ tryptic digestions coupled with imaging mass spectrometry.* Journal of Mass Spectrometry, 2007. **42**(2): p. 254-262.
252. Li, C.M., et al., *Electrochemical detection of nitric oxide on a SWCNT/RTIL composite gel microelectrode.* Electroanalysis: An International Journal Devoted to Fundamental and Practical Aspects of Electroanalysis, 2006. **18**(7): p. 713-718.
253. Hartschuh, A., et al., *Simultaneous fluorescence and Raman scattering from single carbon nanotubes.* Science, 2003. **301**(5638): p. 1354-1356.
254. McCartney, L.J., et al., *Near-infrared fluorescence lifetime assay for serum glucose based on allophycocyanin-labeled concanavalin A.* Analytical Biochemistry, 2001. **292**(2): p. 216-221.
255. Wray, S., et al., *Characterization of the near infrared absorption spectra of cytochrome aa3 and haemoglobin for the non-invasive monitoring of cerebral oxygenation.* Biochimica et Biophysica Acta (BBA)-Bioenergetics, 1988. **933**(1): p. 184-192.
256. Klonis, N., et al., *Characterization of a series of far-red-absorbing thiobarbituric acid oxonol derivatives as fluorescent probes for biological applications.* Analytical biochemistry, 2003. **317**(1): p. 47-58.
257. Kim, S., et al., *Near-infrared fluorescent type II quantum dots for sentinel lymph node mapping.* Nature biotechnology, 2004. **22**(1): p. 93.
258. Pereira, A.N., et al., *Effect of low-power laser irradiation on cell growth and procollagen synthesis of cultured fibroblasts.* Lasers in Surgery and Medicine: The Official Journal of the American Society for Laser Medicine and Surgery, 2002. **31**(4): p. 263-267.
259. Eduardo, F.d.P., et al., *Stem cell proliferation under low intensity laser irradiation: a preliminary study.* Lasers in Surgery and Medicine: The Official Journal of the American Society for Laser Medicine and Surgery, 2008. **40**(6): p. 433-438.
260. Marques, M.M., et al., *Effect of low-power laser irradiation on protein synthesis and ultrastructure of human gingival fibroblasts.* Lasers in surgery and medicine, 2004. **34**(3): p. 260-265.
261. Kruss, S., et al., *Neurotransmitter detection using corona phase molecular recognition on fluorescent single-walled carbon nanotube sensors.* Journal of the American Chemical Society, 2014. **136**(2): p. 713-724.
262. Rusmini, F., Z. Zhong, and J. Feijen, *Protein immobilization strategies for protein biochips.* Biomacromolecules, 2007. **8**(6): p. 1775-1789.
263. Frostell, C., et al., *Inhaled nitric oxide. A selective pulmonary vasodilator reversing hypoxic pulmonary vasoconstriction.* Circulation, 1991. **83**(6): p. 2038-2047.
264. Bogdan, C., *Nitric oxide synthase in innate and adaptive immunity: an update.* Trends in immunology, 2015. **36**(3): p. 161-178.

265. Cossenza, M., et al., *Nitric oxide in the nervous system: biochemical, developmental, and neurobiological aspects*, in *Vitamins & Hormones*. 2014, Elsevier. p. 79-125.
266. Wink, D.A. and J.B. Mitchell, *Nitric oxide and cancer: an introduction.* Free radical biology & medicine, 2003. **34**(8): p. 951-954.
267. Wink, D.A., et al., *The multifaceted roles of nitric oxide in cancer.* Carcinogenesis, 1998. **19**(5): p. 711-721.
268. Lancaster, J.R. and K. Xie, *Tumors face NO problems?* Cancer Research, 2006. **66**(13): p. 6459-6462.
269. Hofseth, L.J., et al., *Nitric oxide in cancer and chemoprevention.* Free Radical Biology and Medicine, 2003. **34**(8): p. 955-968.
270. Hofseth, L.J., *Nitric oxide as a target of complementary and alternative medicines to prevent and treat inflammation and cancer.* Cancer letters, 2008. **268**(1): p. 10-30.
271. Yang, Z., et al., *Streptavidin-Functionalized Three-Dimensional Ordered Nanoporous Silica Film for Highly Efficient Chemiluminescent Immunosensing.* Advanced Functional Materials, 2008. **18**(24): p. 3991-3998.
272. Biotechnology, P., *Instructions HABA 4′-hydroxyazobenzene-2-carboxylic acid*. Thermo Scientific.
273. Qiang, L. and J. Zhou, *Determination of nitric oxide using horseradish peroxidase by UV second-order derivative spectrometry.* Analytical Sciences, 2009. **25**(12): p. 1467-1470.
274. Roxbury, D., et al., *Hyperspectral microscopy of near-infrared fluorescence enables 17-chirality carbon nanotube imaging.* Scientific reports, 2015. **5**: p. 14167.
275. Nakayama-Ratchford, N., et al., *Noncovalent functionalization of carbon nanotubes by fluorescein− polyethylene glycol: supramolecular conjugates with pH-dependent absorbance and fluorescence.* Journal of the American Chemical Society, 2007. **129**(9): p. 2448-2449.
276. Nißler, R., et al., *Quantification of the Number of Adsorbed DNA Molecules on Single-Walled Carbon Nanotubes.* The Journal of Physical Chemistry C, 2019. **123**(8): p. 4837-4847.
277. Sumner, A.L., et al., *The nature of water on surfaces of laboratory systems and implications for heterogeneous chemistry in the troposphere.* Physical Chemistry Chemical Physics, 2004. **6**(3): p. 604-613.
278. Eske, L.D. and D.W. Galipeau, *Characterization of SiO2 surface treatments using AFM, contact angles and a novel dewpoint technique.* Colloids and Surfaces A: Physicochemical and Engineering Aspects, 1999. **154**(1-2): p. 33-51.
279. Wong, A.K. and U.J. Krull, *Surface characterization of 3-glycidoxypropyltrimethoxysilane films on silicon-based substrates.* Analytical and bioanalytical chemistry, 2005. **383**(2): p. 187-200.
280. Qin, M., et al., *Two methods for glass surface modification and their application in protein immobilization.* Colloids and Surfaces B: Biointerfaces, 2007. **60**(2): p. 243-249.
281. Karu, T.I., *Effects of visible radiation on cultured cells.* Photochemistry and photobiology, 1990. **52**(6): p. 1089-1098.

282. Martin, K.J., et al., *A need for basic research on fluid-based early detection biomarkers.* Cancer research, 2010. **70**(13): p. 5203-5206.
283. Anand, S., et al., *Detection and confirmation of serum lipid biomarkers for preeclampsia using direct infusion mass spectrometry.* Journal of lipid research, 2016. **57**(4): p. 687-696.
284. Bhatnagar, D., I. Kaur, and A. Kumar, *Ultrasensitive cardiac troponin I antibody based nanohybrid sensor for rapid detection of human heart attack.* International journal of biological macromolecules, 2017. **95**: p. 505-510.
285. Bala, S., et al., *Increased microRNA-155 expression in the serum and peripheral monocytes in chronic HCV infection.* Journal of translational medicine, 2012. **10**(1): p. 151.
286. Qi, Y., et al., *Altered serum microRNAs as biomarkers for the early diagnosis of pulmonary tuberculosis infection.* BMC infectious diseases, 2012. **12**(1): p. 384.
287. Simon, L., et al., *Serum procalcitonin and C-reactive protein levels as markers of bacterial infection: a systematic review and meta-analysis.* Clinical infectious diseases, 2004. **39**(2): p. 206-217.
288. Mittal, M., et al., *Reactive oxygen species in inflammation and tissue injury.* Antioxidants & redox signaling, 2014. **20**(7): p. 1126-1167.
289. Lefkovits, I. and B. Pernis, *Immunological methods*. Vol. 3. 2014: Elsevier.
290. Chen, C., et al., *Real-time quantification of microRNAs by stem–loop RT–PCR.* Nucleic acids research, 2005. **33**(20): p. e179-e179.
291. Patel, A., et al., *Lipids detection and quantification in oleaginous microorganisms: an overview of the current state of the art.* BMC Chemical Engineering, 2019. **1**(1): p. 13.
292. Sun, J., et al., *Measurement of nitric oxide production in biological systems by using Griess reaction assay.* Sensors, 2003. **3**(8): p. 276-284.
293. Green, N.M., *Avidin*, in *Advances in protein chemistry*. 1975, Elsevier. p. 85-133.
294. Green, N.M., *[5] Avidin and streptavidin*, in *Methods in enzymology*. 1990, Elsevier. p. 51-67.
295. Nguyen, T.T., K.L. Sly, and J.C. Conboy, *Comparison of the energetics of avidin, streptavidin, neutrAvidin, and anti-biotin antibody binding to biotinylated lipid bilayer examined by second-harmonic generation.* Analytical chemistry, 2011. **84**(1): p. 201-208.
296. Dimitrov, A.S. and K. Nagayama, *Continuous convective assembling of fine particles into two-dimensional arrays on solid surfaces.* Langmuir, 1996. **12**(5): p. 1303-1311.
297. Jiang, P., et al., *Single-crystal colloidal multilayers of controlled thickness.* Chemistry of Materials, 1999. **11**(8): p. 2132-2140.
298. Wong, S., V. Kitaev, and G.A. Ozin, *Colloidal crystal films: Advances in universality and perfection.* Journal of the American Chemical Society, 2003. **125**(50): p. 15589-15598.
299. Holland, B.T., C.F. Blanford, and A. Stein, *Synthesis of macroporous minerals with highly ordered three-dimensional arrays of spheroidal voids.* Science, 1998. **281**(5376): p. 538-540.

300. Lytle, J.C. and A. Stein, *Recent progress in syntheses and applications of inverse opals and related macroporous materials prepared by colloidal crystal templating*, in *Annual Review of Nano Research*. 2006, World Scientific. p. 1-79.
301. Velev, O.D. and A.M. Lenhoff, *Colloidal crystals as templates for porous materials.* Current opinion in colloid & interface science, 2000. **5**(1-2): p. 56-63.
302. Xia, Y., et al., *Monodispersed colloidal spheres: old materials with new applications.* Advanced Materials, 2000. **12**(10): p. 693-713.
303. Zhao, X., et al., *Templating methods for preparation of porous structures.* Journal of Materials Chemistry, 2006. **16**(7): p. 637-648.
304. Hatton, B., et al., *Assembly of large-area, highly ordered, crack-free inverse opal films.* Proceedings of the National Academy of Sciences, 2010. **107**(23): p. 10354-10359.
305. Kumar, S., et al., *Biocompatible self-assembled monolayer platform based on (3-glycidoxypropyl) trimethoxysilane for total cholesterol estimation.* Analytical Methods, 2011. **3**(10): p. 2237-2245.
306. Ivanov, A.E., et al., *Affinity Adhesion of Carbohydrate Particles and Yeast Cells to Boronate-Containing Polymer Brushes Grafted onto Siliceous Supports.* Chemistry–A European Journal, 2006. **12**(27): p. 7204-7214.
307. Eslami-Farsani, R., H. Khosravi, and S. Fayazzadeh, *Using-3-glycidoxypropyltrimethoxysilane functionalized SiO2 nanoparticles to improve flexural properties of glass fibers/epoxy grid-stiffened composite panels.* Int. J. Chem. Mol. Nucl. Mater. Metall. Eng, 2015. **9**: p. 1377-1380.
308. Giraldo, J.P., et al., *A Ratiometric Sensor Using Single Chirality Near-Infrared Fluorescent Carbon Nanotubes: Application to In Vivo Monitoring.* Small, 2015. **11**(32): p. 3973-3984.
309. Zhang, X., L. Meng, and Q. Lu, *Cell behaviors on polysaccharide-wrapped single-wall carbon nanotubes: a quantitative study of the surface properties of biomimetic nanofibrous scaffolds.* Acs Nano, 2009. **3**(10): p. 3200-3206.